

1-Bit MIMO for Terahertz Channels

Angel Lozano, *Fellow, IEEE*

Abstract—This paper tackles the problem of single-user multiple-input multiple-output communication with 1-bit digital-to-analog and analog-to-digital converters. With the information-theoretic capacity as benchmark, the complementary strategies of beamforming and equiprobable signaling are contrasted in the regimes of operational interest, and the ensuing spectral efficiencies are characterized. Various canonical channel types are considered, with emphasis on line-of-sight settings under both spherical and planar wavefronts, respectively representative of short and long transmission ranges at mmWave and terahertz frequencies. In all cases, a judicious combination of beamforming and equiprobable signaling is shown to operate within a modest gap from capacity.

I. INTRODUCTION

As they evolve, wireless systems seek to provide ever faster bit rates and lower latencies, and a key enabler for these advances in the increase in bandwidth. From 1G to 5G, the spectrum devoted to wireless communication has surged from a handful of MHz to multiple GHz, roughly three orders of magnitude, and this growth is bound to continue as new mmWave bands open up and inroads are made into the terahertz realm [2]–[6].

Besides bandwidth, another key resource is power. Leaving aside the power spent in duties unrelated to communication, the power consumed by a device can be partitioned as $P_t/\eta + P_{\text{ADC}} + P_{\text{other}}$ where P_t is the power radiated by the transmitter, η is the efficiency of the corresponding power amplifiers, P_{ADC} is the power required by the receiver’s analog-to-digital (ADC) converters, and P_{other} subsumes everything else (including oscillators, filters, the transmitter’s digital-to-analog (DAC) converters, and the receiver’s low-noise amplifier). With B denoting the bandwidth and b the resolution in bits, each ADC satisfies

$$P_{\text{ADC}} = \text{FoM} B \kappa^b \quad (1)$$

where FoM is a figure of merit and κ ranges between two and four [7], [8].

Power consumption has traditionally been dominated by P_t/η and thus high resolutions ($b = 8$ – 12 bits) could be employed. In 1G and 2G, a higher η was facilitated by the adoption of (respectively analog and digital) signaling formats tolerant of nonlinear amplification, but after 2G this took a backseat to spectral efficiency. Linearity has

since reigned, despite the lower η , as P_t/η was well within the power budget of devices for the desirable P_t .

The advent of 5G, with the move up to mmWave frequencies and the enormous bandwidths therein, is a turning point in the sense of P_{ADC} ceasing to be secondary, and this can only accelerate moving forward [9]. Consider this progression: with $b = 10$ at a typical 4G bandwidth of $B = 20$ MHz, P_{ADC} is only a few milliwatts; for $B = 2$ GHz, it is already on the order of a watt; and for $B = 20$ GHz, it would reach roughly 10 watts. Indeed, as B continues to grow, P_{ADC} is bound to swallow up the entire power budget of portable devices unless FoM or b change. But FoM is approaching a fundamental limit [8]. Moreover, while holding steady up to about $B = 100$ MHz, FoM drops sustainably after that mark, which is coincidentally the largest 4G bandwidth. Inevitably then, b has to decrease and, ultimately, it should reach $b = 1$, to drastically curb the power consumption and to further enable dispensing with automatic gain control at the receiver while simplifying the data pipeline between the ADCs and the baseband processing [10].

While 1-bit ADCs curb the spectral efficiency at 1 bit per dimension, the vast bandwidths thereby rendered possible make it exceedingly beneficial. Going from $b = 10$ down to $b = 1$ cuts the spectral efficiency by a factor of 2–3, but in exchange B can grow by as much as 1000 under the same P_{ADC} ; the net benefits in bit rate and latency are stupendous. Spectral efficiency is then best recovered by expanding the number of antennas, which P_{ADC} is only linear in. This naturally leads to multiple-input multiple-output (MIMO) arrangements with 1-bit ADCs.

Although 1-bit ADCs at the receiver do not necessarily entail 1-bit DACs at the transmitter, and in some cases the spectral efficiency could improve somewhat with richer DACs, it is inviting to take the opportunity and adopt 1-bit transmit signals. This not only minimizes the DAC power consumption—somewhat lower than its ADC’s counterpart, yet also considerable [11]–[13]—but it enables the power amplifiers to operate in nonlinear regimes where η is higher.

Altogether, 1-bit MIMO architectures might feature prominently in future wireless systems, and not only for mmWave or terahertz operation: these architectures are also a sensible way forward for lower-frequency extreme massive MIMO, with antenna counts in the hundreds or even thousands [14]. All this interest is evidenced by the extensive literature on transmission strategies and the ensuing performance with 1-bit converters at the transmitter or receiver only (see [15]–[45] and references therein), and by the smaller but growing body of work that considers

A. Lozano is with Univ. Pompeu Fabra, 08018 Barcelona (e-mail: angel.lozano@upf.edu). His work is supported by the European Research Council under the H2020 Framework Programme/ERC grant agreement 694974, by MINECO’s Projects RTI2018-102112 and RTI2018-101040, and by ICREA. Parts of this paper were presented at the 2021 Int’l ITG Workshop on Smart Antennas [1].

1-bit converters at both ends [46]–[59]. Chief among the difficulties in this most stringent case stand (i) computing the information-theoretic performance limits for moderate and large antenna counts, and (ii) precoding to generate signals that can approach those limits.

On these fronts, and concentrating on single-user MIMO, this paper has a two-fold objective:

- To provide analytical characterizations of the performance of beamforming and equiprobable signaling, two transmission strategies that are information-theoretically motivated and complementary.
- To show that a judicious combination of these strategies suffices to operate within a modest gap from the 1-bit capacity in various classes of channels of high relevance, foregoing general precoding solutions.

II. SIGNAL AND CHANNEL MODELS

A. Signal Model

Consider a transmitter equipped with N_t antennas and 1-bit DACs per complex dimension. The receiver, which features N_r antennas and a 1-bit ADC per complex dimension, observes

$$\mathbf{y} = \text{sgn} \left(\sqrt{\frac{\text{SNR}}{2N_t}} \mathbf{H} \mathbf{x} + \mathbf{z} \right) \quad (2)$$

where the sign function is applied separately to the real and imaginary parts of each entry, such that $y_n \in \{\pm 1 \pm j\}$, while \mathbf{H} is the $N_r \times N_t$ channel matrix, $\mathbf{z} \sim \mathcal{N}_{\mathbb{C}}(\mathbf{0}, \mathbf{I})$ is the noise, and SNR is the signal-to-noise ratio per receive antenna. Each entry of the transmit vector \mathbf{x} also takes the values $\pm 1 \pm j$.

Each antenna in the foregoing formulation could actually correspond to a compact subarray, in which case the model subsumes array-of-subarrays structures for the transmitter and/or receiver [60]–[64] provided SNR is appropriately scaled.

For each given \mathbf{H} , the relationship in (2) embodies a discrete memoryless channel with $4^{N_t} \times 4^{N_r}$ transition probabilities determined by

$$p_{\mathbf{y}|\mathbf{x}} = \prod_{n=0}^{N_r-1} p_{\Re\{y_n\}|\mathbf{x}} p_{\Im\{y_n\}|\mathbf{x}}, \quad (3)$$

where the factorization follows from the noise independence per receive antenna and complex dimension. Each such noise component has variance $1/2$, hence

$$p_{\Re\{y_n\}|\mathbf{x}}(1|\mathbf{x}) = \Pr \left[\sqrt{\frac{\text{SNR}}{2N_t}} \Re\{\mathbf{h}_n \mathbf{x} + z_n\} > 0 \right] \quad (4)$$

$$= \Pr \left[\Re\{z_n\} > -\sqrt{\frac{\text{SNR}}{2N_t}} \Re\{\mathbf{h}_n \mathbf{x}\} \right] \quad (5)$$

$$= Q \left(-\sqrt{\frac{\text{SNR}}{N_t}} \Re\{\mathbf{h}_n \mathbf{x}\} \right) \quad (6)$$

where \mathbf{h}_n is the n th row of \mathbf{H} (for $n = 0, \dots, N_r - 1$) and $Q(\cdot)$ is the Gaussian Q-function. Similarly,

$$p_{\Re\{y_n\}|\mathbf{x}}(-1|\mathbf{x}) = Q \left(\sqrt{\frac{\text{SNR}}{N_t}} \Re\{\mathbf{h}_n \mathbf{x}\} \right). \quad (7)$$

From (6) and (7),

$$p_{\Re\{y_n\}|\mathbf{x}}(\Re\{y_n\}|\mathbf{x}) = Q \left(-\Re\{y_n\} \sqrt{\frac{\text{SNR}}{N_t}} \Re\{\mathbf{h}_n \mathbf{x}\} \right) \quad (8)$$

and, mirroring it, finally

$$p_{\mathbf{y}|\mathbf{x}}(\mathbf{y}|\mathbf{x}) = \prod_{n=0}^{N_r-1} Q \left(-\Re\{y_n\} \sqrt{\frac{\text{SNR}}{N_t}} \Re\{\mathbf{h}_n \mathbf{x}\} \right) \cdot Q \left(-\Im\{y_n\} \sqrt{\frac{\text{SNR}}{N_t}} \Im\{\mathbf{h}_n \mathbf{x}\} \right). \quad (9)$$

The transition probabilities correspond to (9) evaluated for the 4^{N_r} possible values of \mathbf{y} and the 4^{N_t} values of \mathbf{x} . If \mathbf{H} is known, these transition probabilities can be readily computed. Conversely, if the transition probabilities are known, \mathbf{H} can be deduced.

The 4^{N_t} transmit vectors \mathbf{x} can be partitioned into 4^{N_t-1} quartets, each containing four vectors and being invariant under a 90° phase rotation of all the entries: from any vector in the quartet, the other three are obtained by repeatedly multiplying by j . Since a 90° phase rotation of \mathbf{x} propagates as a 90° phase rotation of $\mathbf{H}\mathbf{x}$, and the added noise is circularly symmetric, the four vectors making up each transmit quartet are statistically equivalent and they should thus have the same transmission probability so as to convey the maximum amount of information.

Likewise, the set of 4^{N_r} possible vectors \mathbf{y} can be partitioned into 4^{N_r-1} quartets, and the four vectors \mathbf{y} within each received quartet are equiprobable.

B. Channel Model

If the channel is stable over each codeword, then every realization of \mathbf{H} has operational significance and SNR is well defined under the normalization $\text{tr}(\mathbf{H}\mathbf{H}^*) = N_t N_r$. Conversely, if the coding takes place over a sufficiently broad range of channel fluctuations, that significance is acquired in an ergodic sense with $\mathbb{E}[\text{tr}(\mathbf{H}\mathbf{H}^*)] = N_t N_r$ [65]. The following classes of channels are specifically considered.

a) Line-of-Sight (LOS) with Spherical Wavefronts:

LOS is the chief propagation mechanism at mmWave and terahertz frequencies, and the spherical nature of the wavefronts is relevant for large arrays and short transmission ranges. For uniform linear arrays (ULAs) [66],

$$\mathbf{H} = \mathbf{D}_{\text{rx}} \tilde{\mathbf{H}} \mathbf{D}_{\text{tx}} \quad (10)$$

where \mathbf{D}_{rx} and \mathbf{D}_{tx} are diagonal matrices with entries

$$\begin{aligned} [\mathbf{D}_{\text{rx}}]_{n,n} &= e^{-j\pi \left[\frac{2n}{\lambda} d_r \sin \theta_r \cos \phi + \frac{n^2}{\lambda D} d_r^2 (1 - \sin^2 \theta_r \cos^2 \phi) \right]} \\ [\mathbf{D}_{\text{tx}}]_{m,m} &= e^{-j\pi \left[\frac{2m}{\lambda} d_t \sin \theta_t + \frac{m^2}{\lambda D} d_t^2 \right]} \end{aligned} \quad (11)$$

and with D the range, λ the wavelength, d_t and d_r the antenna spacings at transmitter and receiver, θ_t and θ_r the transmitter and receiver elevations, and ϕ their relative azimuth angle. In turn, $\tilde{\mathbf{H}}$ is the Vandermonde matrix

$$\tilde{\mathbf{H}} = \begin{bmatrix} e^{j2\pi\eta\frac{0 \times 0}{N_{\max}}} & \dots & e^{j2\pi\eta\frac{(N_t-1) \times 0}{N_{\max}}} \\ \vdots & \ddots & \vdots \\ e^{j2\pi\eta\frac{0 \times (N_r-1)}{N_{\max}}} & \dots & e^{j2\pi\eta\frac{(N_t-1) \times (N_r-1)}{N_{\max}}} \end{bmatrix} \quad (12)$$

where $N_{\max} = \max(N_t, N_r)$ while

$$\eta = \frac{(d_r \cos \theta_r)(d_t \cos \theta_t)N_{\max}}{\lambda D} \quad (13)$$

is a parameter that concisely describes any LOS setting with ULAs.

Uniform rectangular arrays can be expressed as the Kronecker product of ULAs, and expressions deriving from (10) emerge [67]. For more complex topologies, the entries of \mathbf{H} continue to be of unit magnitude, but the pattern of phase variations becomes more cumbersome.

b) LOS with Planar Wavefronts: For long enough transmission ranges, the planar wavefront counterpart to (10) is obtained by letting $D \rightarrow \infty$, whereby the channel becomes rank-1 with

$$h_{n,m} = e^{-j\frac{2\pi}{\lambda}(nd_r \sin \theta_r \cos \phi + md_t \sin \theta_t)}. \quad (14)$$

c) IID Rayleigh Fading: In this model, representing situations of rich multipath propagation, the entries of \mathbf{H} are IID and $h_{n,m} \sim \mathcal{N}_{\mathbb{C}}(0, 1)$.

We note that the frequency-flat representation embodied by \mathbf{H} is congruous for the two LOS channel models, but less so for the IID model, where the scattering would go hand in hand with frequency selectivity over the envisioned bandwidths. The analysis presented for this model intends to set the stage for more refined characterizations that account for the inevitable intersymbol interference. In fact, even for the LOS channels, over a sufficiently broad bandwidth there is bound to be intersymbol interference because of spatial widening, i.e., because of the distinct propagation delays between the various transmit and receive antennas [68], [69].

III. 1-BIT CAPACITY

Denote by $p_1, \dots, p_{4^{N_t-1}}$ the activation probabilities of the transmit quartets, such that $\sum_k p_k = 1$ and $p_{\mathbf{x}}(\mathbf{x}_k) = p_k/4$ with \mathbf{x}_k any of the vectors in the k th quartet. Letting $\mathcal{H}(\cdot)$ indicate entropy, and with all the probabilities conditioned on \mathbf{H} , the mutual information is

$$\mathcal{I}(\text{SNR}, \mathbf{H}) = \mathcal{H}(\mathbf{y}) - \mathcal{H}(\mathbf{y}|\mathbf{x}) \quad (15)$$

$$= \sum_{\ell=1}^{4^{N_r}} p_{\mathbf{y}}(\mathbf{y}_{\ell}) \log_2 \frac{1}{p_{\mathbf{y}}(\mathbf{y}_{\ell})} - \mathcal{H}(\mathbf{y}|\mathbf{x}) \quad (16)$$

$$= 4 \sum_{\ell=1}^{4^{N_r-1}} p_{\mathbf{y}}(\mathbf{y}_{\ell}) \log_2 \frac{1}{p_{\mathbf{y}}(\mathbf{y}_{\ell})} - \mathcal{H}(\mathbf{y}|\mathbf{x}) \quad (17)$$

where (17) follows from the equiprobability of the vectors in each received quartet and \mathbf{y}_{ℓ} is any of the vectors in the ℓ th such quartet while

$$p_{\mathbf{y}}(\mathbf{y}) = \sum_{k=1}^{4^{N_t-1}} \frac{p_k}{4} \sum_{i=0}^3 p_{\mathbf{y}|\mathbf{x}}(\mathbf{y}|j^i \mathbf{x}_k) \quad (18)$$

with $p_{\mathbf{y}|\mathbf{x}}$ depending on SNR and \mathbf{H} as per (9). Elaborating on (18),

$$\begin{aligned} p_{\mathbf{y}}(\mathbf{y}) &= \sum_{k=1}^{4^{N_t-1}} \frac{p_k}{4} \left[\prod_{n=0}^{N_r-1} Q\left(-\Re\{y_n\} \sqrt{\frac{\text{SNR}}{N_t}} \Re\{\mathbf{h}_n \mathbf{x}_k\}\right) \right. \\ &\quad \cdot Q\left(-\Im\{y_n\} \sqrt{\frac{\text{SNR}}{N_t}} \Im\{\mathbf{h}_n \mathbf{x}_k\}\right) \\ &\quad + \prod_{n=0}^{N_r-1} Q\left(\Re\{y_n\} \sqrt{\frac{\text{SNR}}{N_t}} \Re\{\mathbf{h}_n \mathbf{x}_k\}\right) \\ &\quad \cdot Q\left(-\Im\{y_n\} \sqrt{\frac{\text{SNR}}{N_t}} \Re\{\mathbf{h}_n \mathbf{x}_k\}\right) \\ &\quad + \prod_{n=0}^{N_r-1} Q\left(\Re\{y_n\} \sqrt{\frac{\text{SNR}}{N_t}} \Re\{\mathbf{h}_n \mathbf{x}_k\}\right) \\ &\quad \cdot Q\left(\Im\{y_n\} \sqrt{\frac{\text{SNR}}{N_t}} \Im\{\mathbf{h}_n \mathbf{x}_k\}\right) \\ &\quad + \prod_{n=0}^{N_r-1} Q\left(-\Re\{y_n\} \sqrt{\frac{\text{SNR}}{N_t}} \Im\{\mathbf{h}_n \mathbf{x}_k\}\right) \\ &\quad \left. \cdot Q\left(\Im\{y_n\} \sqrt{\frac{\text{SNR}}{N_t}} \Re\{\mathbf{h}_n \mathbf{x}_k\}\right) \right]. \quad (19) \end{aligned}$$

In turn, because of the factorization of $p_{\mathbf{y}|\mathbf{x}}$ in (9),

$$\mathcal{H}(\mathbf{y}|\mathbf{x}) = \sum_{n=0}^{N_r-1} (\mathcal{H}(\Re\{y_n\}|\mathbf{x}) + \mathcal{H}(\Im\{y_n\}|\mathbf{x})) \quad (20)$$

$$\begin{aligned} &= \sum_{k=1}^{4^{N_t-1}} \frac{p_k}{4} \sum_{i=0}^3 \sum_{n=0}^{N_r-1} (\mathcal{H}(\Re\{y_n\}|\mathbf{x} = j^i \mathbf{x}_k) \\ &\quad + \mathcal{H}(\Im\{y_n\}|\mathbf{x} = j^i \mathbf{x}_k)) \quad (21) \end{aligned}$$

$$\begin{aligned} &= \sum_{k=1}^{4^{N_t-1}} \frac{p_k}{4} \sum_{i=0}^3 \sum_{n=0}^{N_r-1} \left[\mathcal{H}_b\left(Q\left(-\sqrt{\frac{\text{SNR}}{N_t}} \Re\{\mathbf{h}_n j^i \mathbf{x}_k\}\right)\right) \right. \\ &\quad \left. + \mathcal{H}_b\left(Q\left(-\sqrt{\frac{\text{SNR}}{N_t}} \Im\{\mathbf{h}_n j^i \mathbf{x}_k\}\right)\right) \right] \quad (22) \end{aligned}$$

where $\mathcal{H}_b(p) = -p \log_2 p - (1-p) \log_2 (1-p)$ is the binary entropy function. Since changing i merely flips the sign of some of the Q-function arguments, and $Q(-\xi) = 1 - Q(\xi)$ such that $\mathcal{H}_b(Q(-\xi)) = \mathcal{H}_b(Q(\xi))$, it follows that

$$\begin{aligned} \mathcal{H}(\mathbf{y}|\mathbf{x}) &= \sum_{k=1}^{4^{N_t-1}} p_k \sum_{n=0}^{N_r-1} \left[\mathcal{H}_b\left(Q\left(-\sqrt{\frac{\text{SNR}}{N_t}} \Re\{\mathbf{h}_n \mathbf{x}_k\}\right)\right) \right. \\ &\quad \left. + \mathcal{H}_b\left(Q\left(-\sqrt{\frac{\text{SNR}}{N_t}} \Im\{\mathbf{h}_n \mathbf{x}_k\}\right)\right) \right]. \quad (23) \end{aligned}$$

The combination of (17), (19), and (23) gives $\mathcal{I}(\text{SNR}, \mathbf{H})$, whose evaluation involves $\mathcal{O}(4^{N_t-1} 4^{N_r-1})$

$$S_0 = \frac{2 [\dot{\mathcal{I}}(0)]^2}{-\ddot{\mathcal{I}}(0) \log_2 e} = \frac{\mathbb{E}[\text{tr}(\mathbf{H}\boldsymbol{\Sigma}_{\mathbf{x}}\mathbf{H}^*)]^2}{\frac{1}{2} \mathbb{E}[\text{tr}((\text{nondiag}(\mathbf{H}\boldsymbol{\Sigma}_{\mathbf{x}}\mathbf{H}^*))^2)] + \frac{\pi-1}{3} \mathbb{E}[\|\Re\{\mathbf{H}\mathbf{x}\}\|_4^4 + \|\Im\{\mathbf{H}\mathbf{x}\}\|_4^4]} \quad (29)$$

terms. This becomes prohibitive even for modest N_t and N_r , hence the interest in analytical characterizations. From $\mathcal{I}(\text{SNR}, \mathbf{H})$, the 1-bit capacity is

$$C(\text{SNR}, \mathbf{H}) = \max_{\{p_k\}: \sum_k p_k = 1} \mathcal{I}(\text{SNR}, \mathbf{H}) \quad (24)$$

with maximization over p_1, \dots, p_{4N_t-1} . Since $\mathcal{I}(\text{SNR}, \mathbf{H})$ is concave in p_1, \dots, p_{4N_t-1} and these probabilities define a convex set, (24) can be solved with off-the-shelf convex optimization tools. Or, the Blahut-Arimoto algorithm that alternatively maximizes $p_{\mathbf{x}}$ and $p_{\mathbf{x}|\mathbf{y}}$ can be applied, with converge guarantees to any desired accuracy [70], [71].

In ergodic settings, what applies is the ergodic spectral efficiency

$$\mathcal{I}(\text{SNR}) = \mathbb{E}_{\mathbf{H}}[\mathcal{I}(\text{SNR}, \mathbf{H})] \quad (25)$$

and likewise for the ergodic capacity. Alternatively, if the channel is stable over each codeword, then $\mathcal{I}(\text{SNR}, \mathbf{H})$ and $C(\text{SNR}, \mathbf{H})$ themselves are meaningful for each \mathbf{H} .

The 1-bit capacity cannot exceed $2 \min(N_t, N_r)$ b/s/Hz, with three distinct regimes:

- Low SNR. This is a key regime at mmWave and terahertz frequencies, given the difficulty in producing strong signals, the high propagation losses, and the noise bandwidth.
- Intermediate SNR. Here, the spectral efficiency improves sustainedly with the SNR.
- High SNR. This is a regime of diminishing returns, once the capacity nears $2 \min(N_t, N_r)$.

A. Low SNR

The low-SNR behavior is most conveniently examined with the mutual information expressed as function of the normalized energy per bit at the receiver,

$$\frac{E_b}{N_0} = \frac{\text{SNR}}{\mathcal{I}(\text{SNR})}. \quad (26)$$

Beyond the minimum required value of

$$\frac{E_b}{N_0 \min} = \lim_{\text{SNR} \rightarrow 0} \frac{\text{SNR}}{\mathcal{I}(\text{SNR})}, \quad (27)$$

the mutual information behaves as [72, sec. 4.2]

$$S_0 \frac{\frac{E_b}{N_0} \Big|_{\text{dB}} - \frac{E_b}{N_0 \min} \Big|_{\text{dB}}}{3 \text{ dB}} + \varepsilon, \quad (28)$$

where ε is a lower-order term, S_0 is the slope at $\frac{E_b}{N_0 \min}$ in b/s/Hz/(3 dB), and $z|_{\text{dB}} = 10 \log_{10} z$.

$\frac{E_b}{N_0 \min}$ and S_0 descend from the first and second derivatives of $\mathcal{I}(\text{SNR})$ at $\text{SNR} = 0$, which themselves emerge from (17), (19), and (23) after a tedious derivation [29],

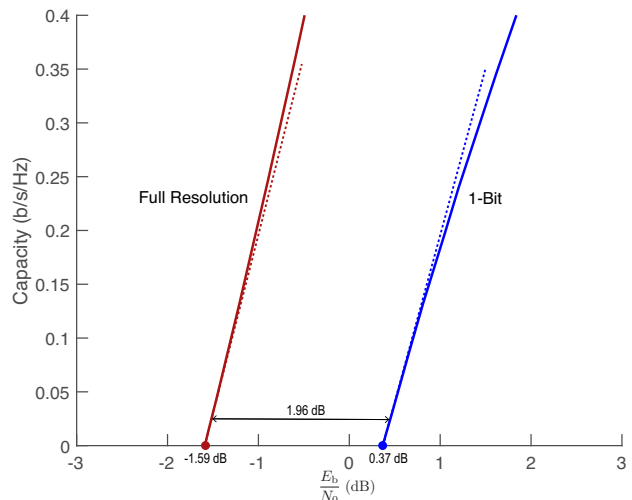


Fig. 1: Capacity as a function of E_b/N_0 for $N_t = N_r = 1$ and Rayleigh fading. The solid lines are the exact capacities (1-bit and full resolution) while the dotted lines represent their respective expansions as per (28).

[31]. Plugging these two derivatives into the definitions of $\frac{E_b}{N_0 \min}$ and S_0 [72, sec. 4.2],

$$\frac{E_b}{N_0 \min} = \frac{1}{\dot{\mathcal{I}}(0)} = \frac{\pi N_t}{\mathbb{E}[\text{tr}(\mathbf{H}\boldsymbol{\Sigma}_{\mathbf{x}}\mathbf{H}^*)] \log_2 e} \quad (30)$$

with $\boldsymbol{\Sigma}_{\mathbf{x}} = \mathbb{E}[\mathbf{x}\mathbf{x}^*] = \sum_k p_k \mathbf{x}_k \mathbf{x}_k^*$, while S_0 equals (29) where $\text{nondiag}(\cdot)$ returns a matrix with its diagonal entries set to zero and $\|\cdot\|_4$ denotes L4 norm.

The expectations in (30) and (29) are conditioned on \mathbf{H} when there is operational significance attached to a specific such value, and unconditioned in the ergodic case.

A worthwhile exercise is to appraise the expansion in (28) against its exact counterpart, a contrast that Fig. 1 presents for $N_t = N_r = 1$ in Rayleigh fading. The characterization provided by (28) is indeed precise, a fact that extends to all other channels considered in the paper.

B. Intermediate SNR

In 1-bit communication, the intermediate-SNR regime steals relevance from its high-SNR counterpart, which becomes unappealing. In order to delineate the reach of this intermediate-SNR regime, it is of interest to establish the limiting capacity for $\text{SNR} \rightarrow \infty$. Let us define

$$C_\infty(\mathbf{H}) = \lim_{\text{SNR} \rightarrow \infty} C(\text{SNR}, \mathbf{H}) \quad (31)$$

and consider channels satisfying $\mathbf{h}_n \mathbf{x} \neq 0$ with probability 1 for $n = 0, \dots, N_r - 1$, such that the transition probabilities have a positive mass only at 0 and 1, meaning that \mathbf{y} is fully determined by \mathbf{x} . The vast majority of channels abide by the condition, and in particular the ones set forth in Sec. II-B.

For $N_t = 1$, a single quartet is available for transmission and, by virtue of its four equiprobable constituent vectors, $C_\infty(\mathbf{H}) = 2$. For $N_t > 1$ and $N_r = 1$, it can be verified that (24) is maximized when a single quartet is activated, depending on \mathbf{H} [57]. Again, $C_\infty(\mathbf{H}) = 2$.

For $N_t > 1$ and $N_r > 1$, it must hold that $C_\infty \leq 2N_t$, but this bound is generally not achievable because some vectors \mathbf{x} map to the same receive vector \mathbf{y} [46]. As the transition probabilities are either 0 or 1, every binary entropy function in (23) vanishes and $\mathcal{H}(\mathbf{y}|\mathbf{x}) \rightarrow 0$, hence the mutual information comes to equal $\mathcal{H}(\mathbf{y})$. Letting

$$\mathcal{Y}(\mathbf{H}) = \left\{ \mathbf{y} \mid \mathbf{y} = \text{sgn}(\mathbf{H}\mathbf{x}) \forall \mathbf{x} \in \{\pm 1 \pm j\}^{N_t} \right\} \quad (32)$$

denote the set of vectors \mathbf{y} that can be elicited for channel \mathbf{H} , the maximization of $\mathcal{H}(\mathbf{y})$ occurs when this set is equiprobable. Then,

$$C_\infty(\mathbf{H}) = \log_2 |\mathcal{Y}(\mathbf{H})| \quad (33)$$

with $\mathbb{E}[C_\infty(\mathbf{H})]$ being the limiting ergodic capacity.

The evaluation of (33) is far simpler than that of $C(\text{SNR})$ in its full generality.

IV. 1-BIT VS FULL-RESOLUTION CAPACITY

A naïve comparison of the 1-bit and full-resolution capacities would indicate that the former always trails the latter. In terms of power, their gap in dB is at least the difference between their $\frac{E_b}{N_{0 \min}}|_{\text{dB}}$ values; in a scalar Rayleigh-faded channel, for instance, what separates the full-resolution mark of -1.59 dB [72, sec. 4.2] from its 1-bit brethren of 0.37 dB is 1.96 dB as noted in Fig. 1. As shall be seen in the sequel, this gap remains rather steady with MIMO and over a variety of channels.

Such naïve comparison, however, only accounts for radiated power, disregarding any other differences in power consumption between the full-resolution and 1-bit alternatives. While appropriate when the radiated power dominates, this neglect becomes misleading when the digitalization consumes sizeable power and, since this is the chief motivation for 1-bit communication, by definition the comparison is somewhat deceptive.

Indeed, whenever the excess power of a full-resolution architecture, relative to 1-bit, exceeds a 1.96 -dB backoff in P_t/η , there is going to be a range of SNRs over which, under a holistic accounting of power, the 1-bit capacity is actually higher. For a very conservative assessment of this phenomenon, let us assume that $\kappa = 2$ in (1) and that η , FoM, and P_{other} , are not affected by the resolution—in actuality all of these quantities shall be markedly better in the 1-bit case—to obtain the condition

$$\frac{1}{10^{1.96/10}} \frac{P_t}{\eta} + \text{FoM} B 2^{11} \geq \frac{P_t}{\eta} + \text{FoM} B 4 \quad (34)$$

where we considered two ADCs ($N_r = 1$) and $b = 10$ bits for full resolution. The above yields

$$B \geq \frac{0.36 P_t/\eta}{\text{FoM}(2^{11} - 4)}, \quad (35)$$

which, for the sensible values $P_t = 23$ dBm and $\eta = 0.4$, and with a state-of-the-art FoM = 10 pJ/conversion [8], evaluates to $B \geq 8.8$ GHz. This highly conservative threshold drops rapidly as the number of digitally processed antennas grows large and thus, for bandwidths well within the scope of upcoming wireless systems, 1-bit MIMO can be viewed as information-theoretically optimum for at least some range of SNRs.

V. TRANSMIT BEAMFORMING

Transmit beamforming corresponds to $\Sigma_{\mathbf{x}}$ being rank-1, i.e., to \mathbf{x} being drawn from a single quartet, with such quartet generally dependent on \mathbf{H} . We examine this strategy with an ergodic perspective; for nonergodic channels, the formulation stands without the expectations over \mathbf{H} .

A. Low SNR

For vanishing SNR, transmit beamforming is not only conceptually appealing, but information-theoretically optimum. Indeed, (30) can be rewritten as

$$\frac{E_b}{N_{0 \min}} = \frac{\pi N_t}{\mathbb{E}[\sum_k p_k \|\mathbf{H}\mathbf{x}_k\|^2] \log_2 e}, \quad (36)$$

which is maximized by assigning probability 1 to the quartet $k^* = \arg \max \|\mathbf{H}\mathbf{x}_k\|^2$ for each realization of \mathbf{H} . Therefore, it is optimum to beamform, and the optimum beamforming quartet is the one maximizing the received power. The task is then to determine k^* from within the 4^{N_t-1} possible quartets.

For $N_t = 1$, there is no need to optimize over k —only one quartet can be transmitted—and thus

$$\frac{E_b}{N_{0 \min}} = \frac{\pi}{2N_r \log_2 e}, \quad (37)$$

which amounts to 0.37 dB for $N_r = 1$ [73] and improves by 3 dB with every doubling of N_r thereafter.

For $N_t > 1$, it is useful to recognize that the choices for \mathbf{x} that are bound to yield high values for $\|\mathbf{H}\mathbf{x}\|^2$ are those that project maximally on the dimension of \mathbf{H} that offers the largest gain, namely the maximum-eigenvalue eigenvector of $\mathbf{H}^* \mathbf{H}$. This, in turn, requires that \mathbf{x} mimic, as best as possible, the structure of that eigenvector; since the magnitude of the entries of \mathbf{x} is fixed, this mimicking ought to be in terms of phases only. Formalizing this intuition, it is possible to circumvent the need to exhaustively search the entire field of 4^{N_t-1} possibilities and conveniently identify a subset of only N_t quartet candidates that is sure to contain the one best aligning with the maximum-eigenvalue eigenvector of $\mathbf{H}^* \mathbf{H}$, denoted henceforth by \mathbf{v}_0 . Precisely, as detailed in Appendix A, if we let $\varphi_m = \angle(\mathbf{v}_{0,m}) + \epsilon$ for $m = 0, \dots, N_t - 1$, the N_t quartets in the subset can be determined as

$$\mathbf{x}_k = \text{sgn}(e^{j\varphi_{k-1}} \mathbf{v}_0) \quad k = 1, \dots, N_t \quad (38)$$

where ϵ is a small quantity, positive or negative. If the channel is rank-1, then this subset is sure to contain the optimum \mathbf{x}_{k^*} ; if the rank is higher, then optimality is not

guaranteed, but the best value in the above subset is bound to yield excellent performance.

Turning to the $\frac{E_b}{N_0 \min}$ achieved by \mathbf{x}_{k^*} , its explicit evaluation is complicated, yet its value can be shown (see Appendix A again) to satisfy

$$\frac{\pi}{2 \mathbb{E}[\lambda_0] \log_2 e} \leq \frac{E_b}{N_0 \min} \leq \frac{\pi^3 N_t}{16 \mathbb{E}[\lambda_0 \|\mathbf{v}_0\|_1^2] \log_2 e} \quad (39)$$

where λ_0 is the maximum eigenvalue of $\mathbf{H}^* \mathbf{H}$ while $\|\cdot\|_1$ denotes L1 norm. For $N_r = 1$, (39) specializes to

$$\frac{\pi}{2 N_t \log_2 e} \leq \frac{E_b}{N_0 \min} \leq \frac{\pi^3}{16 (1 + (N_t - 1) \frac{\pi}{4}) \log_2 e}.$$

Finally, S_0 can be obtained by plugging $\mathbf{x} = \mathbf{x}_{k^*}$ and $\Sigma_{\mathbf{x}} = \mathbf{x}_{k^*} \mathbf{x}_{k^*}^*$ into (29).

B. Intermediate SNR

The low-SNR linearity of the mutual information in the received power is the root cause of the optimality of power-based beamforming in that regime. The orientation on the complex plane of the received signals is immaterial—a rotation shifts power from the real to the imaginary part, or vice versa, but the total power is preserved. Likewise, the power split among receive antennas is immaterial to the low-SNR mutual information.

At higher SNRs, the linearity breaks down and the mutual information becomes a more intricate function of $\mathbf{H}\mathbf{x}$, such that proper signal orientations and power balances become important, to keep $\mathbf{h}_n \mathbf{x}$ away from the ADC quantization boundaries for $n = 0, \dots, N_r - 1$. This has a dual consequence:

- Transmit beamforming ceases to be generally optimum, even if the channel is rank-1.
- Even within the confines of beamforming, solutions not based on maximizing power are more satisfying.

As exemplified in Fig. 2 for $N_r = 1$, a beamforming quartet with a better complex-plane disposition at the receiver may be preferable to one yielding a larger magnitude. This is because, after a 1-bit ADC, only 90° rotations and no scalings are possible (in contrast with full-resolution receivers, where $\mathbf{h}\mathbf{x}$ can subsequently be rotated and scaled). The best beamforming quartet is the one that simultaneously ensures large real and imaginary parts for $\mathbf{h}_n \mathbf{x}$ in a balanced fashion for $n = 0, \dots, N_r - 1$, and the task of identifying this quartet is a fitting one for learning algorithms [58], [74].

We note that, with full-resolution converters, multiple receive antennas play a role dual to that of transmit beamforming [72, sec. 5.3], and the spectral efficiency with N transmit and one receive antenna equals its brethren with one transmit and N receive antennas. With 1-bit converters, in contrast, transmit beamforming optimizes $\mathbf{h}_n \mathbf{x}$ for $n = 0, \dots, N_r - 1$, to mitigate the addition of noise prior to quantization, while multiple receive antennas yield a diversity of quantized observations from which better decisions can be made on which of the possible vectors was transmitted. This includes majority decisions and erasure declarations in the case of split observations.



Fig. 2: Complex plane representation of the four values of $\mathbf{h}\mathbf{x}$ for a given \mathbf{h} and a given quartet, with the ADC quantization boundaries indicated by dashed lines. Left-hand side, for \mathbf{x}_k , which has a larger magnitude but worse orientation. Right-hand side, for \mathbf{x}_ℓ , which has a smaller magnitude but better orientation. On this channel, quartet k yields a higher mutual at low SNR while quartet ℓ yields a higher mutual information beyond the low-SNR regime.

VI. EQUIPROBABLE SIGNALING

The complementary strategy to beamforming is to activate multiple quartets, increasing the rank of $\Sigma_{\mathbf{x}}$. Ultimately, all quartets can be activated with equal probability, such that $\Sigma_{\mathbf{x}} = 2\mathbf{I}$. This renders the signals IID across the transmit antennas, i.e., pure spatial multiplexing. We examine this strategy with an ergodic perspective.

A. Low SNR

With equiprobable signaling, (30) gives

$$\frac{E_b}{N_0 \min} = \frac{\pi}{2 N_r \log_2 e}. \quad (40)$$

In addition [31],

$$\mathbb{E}_{\mathbf{x}} [\|\Re\{\mathbf{H}\mathbf{x}\}\|_4^4 + \|\Im\{\mathbf{H}\mathbf{x}\}\|_4^4] = 6 \text{tr}((\text{diag}(\mathbf{H}\mathbf{H}^*))^2) - 4 \sum_{n=0}^{N_r-1} \sum_{m=0}^{N_t-1} (\Re\{h_{n,m}\}^4 + \Im\{h_{n,m}\}^4), \quad (41)$$

based on which S_0 in (29) simplifies considerably.

Combining (39) and (40), the low-SNR advantage of optimum beamforming over equiprobable signaling, denoted by Δ_{BF} , is tightly bounded as

$$\frac{8 \mathbb{E}[\lambda_0 \|\mathbf{v}_0\|_1^2]}{\pi^2 N_t N_r} \leq \Delta_{\text{BF}} \leq \frac{\mathbb{E}[\lambda_0]}{N_r}. \quad (42)$$

This enables some general considerations:

- The low-SNR advantage of beamforming is essentially determined by the maximum eigenvalue of $\mathbf{H}^* \mathbf{H}$. The advantage is largest in rank-1 channels, and minimal if all eigenvalues are equal (on average or instantaneously, as pertains to ergodic and nonergodic settings).
- If all eigenvalues are equal, beamforming may still yield a lingering advantage for $N_t > N_r$, but not otherwise. Indeed, for $N_t \leq N_r$, if all eigenvalues all equal then $\mathbb{E}[\lambda_0] = N_r$ and thus $\Delta_{\text{BF}} \leq 1$.

B. Intermediate SNR

While beamforming is optimum at low SNR, it is decidedly suboptimum beyond, and activating multiple quartets becomes instrumental to surpass the 2-b/s/Hz

mark. This is the case even in rank-1 channels, where the activation of multiple quartets allows producing richer signals; this can be seen as the 1-bit counterpart to higher-order constellations. And, given how the curse of dimensionality afflicts the computation of the optimum quartet probabilities, equiprobable signaling is a very enticing way of going about this. As will be seen, not only is it implementationally convenient, but highly effective.

VII. CHANNELS OF INTEREST

Capitalizing on the analytical tools set forth hitherto, let us now examine the performance of transmit beamforming and equiprobable signaling in various classes of channels, starting with the nonergodic LOS settings and progressing on to the ergodic IID Rayleigh-faded channel.

A. LOS with Planar Wavefronts

This channel is rank-1, hence the optimum $\frac{E_b}{N_0 \min}$ can be achieved with equality by the best beamforming quartet in subset (38). More conveniently for our purposes here, we can rewrite (10) as $\mathbf{H} = \sqrt{N_t N_r} \mathbf{u} \mathbf{v}^*$ where

$$u_n = \frac{1}{\sqrt{N_r}} e^{-j\pi \frac{2n}{\lambda} d_r \sin\theta_r \cos\phi} \quad (43)$$

$$v_m = \frac{1}{\sqrt{N_t}} e^{-j\pi \frac{2m}{\lambda} d_t \sin\theta_t}. \quad (44)$$

Irrespective of the array orientations, $\lambda_0 = N_t N_r$ and $\|\mathbf{v}_0\|_1^2 = N_t$ such that (39) reverts to

$$\frac{\pi}{2 N_t N_r \log_2 e} \leq \frac{E_b}{N_0 \min} \leq \frac{\pi^3}{16 N_t N_r \log_2 e}, \quad (45)$$

which depends symmetrically on N_t and N_r . The significance of $\frac{E_b}{N_0 \min}$ as the key measure of low-SNR performance can be appreciated in Fig. 3, which depicts the low-SNR capacity as a function of $\frac{E_b}{N_0}$ for $N_t = N_r = 1, 2,$ and 4 in an exemplary LOS setting. Adding antennas essentially displaces the capacity by the amount by which $\frac{E_b}{N_0 \min}$ changes.

Shown in Fig. 4 is how $\frac{E_b}{N_0 \min}$ improves with the number of antennas ($N_t = N_r$) for the same setting. Also shown are the values for equiprobable signaling, undesirable in this case as per (42). The low-SNR advantage of beamforming accrues steadily with the numbers of antennas and the bounds in (39) tightly bracket the optimum $\frac{E_b}{N_0 \min}$. As anticipated, the gap of 1-bit beamforming to full-resolution beamforming (included in the figure) remains small.

Moving up to intermediate SNRs, the beamforming and equiprobable-signaling performance on another setting is presented in Fig. 5. Also shown is the actual capacity with $p_1, \dots, p_{4^{N_t-1}}$ optimized via Blahut-Arimoto. Up to when the 2-b/s/Hz ceiling is approached, beamforming performs splendidly. Past that level, and no matter the rank-1 nature of the channel, equiprobable signaling is highly superior, tracking the capacity to within a roughly constant shortfall. This example represents well the intermediate-SNR performance in planar-wavefront LOS channels, a

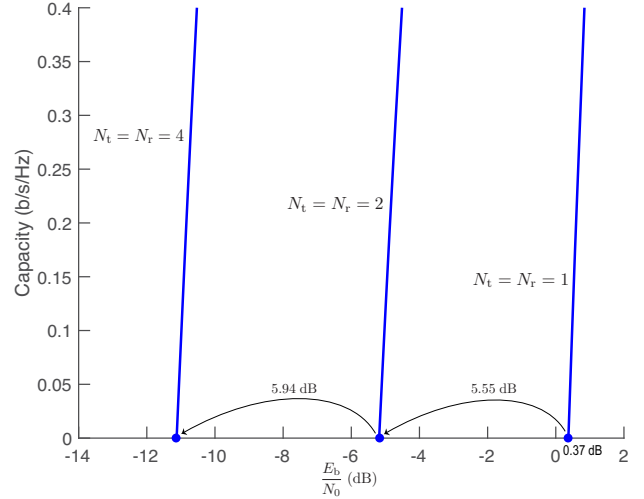


Fig. 3: Capacity as a function of E_b/N_0 for $N_t = N_r = 1, N_t = N_r = 2,$ and $N_t = N_r = 4,$ in a planar-wavefront LOS channel with half-wavelength antenna spacings, $\theta_t = 0,$ $\theta_r = \pi/6,$ and $\phi = \pi/4.$

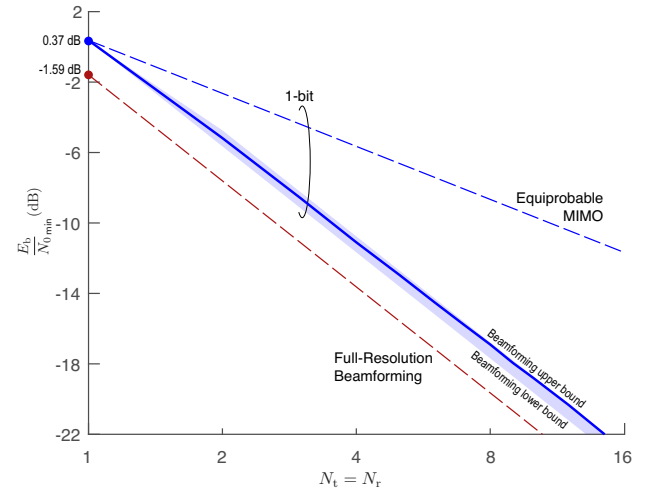


Fig. 4: Minimum E_b/N_0 as a function of $N_t = N_r$ for a planar-wavefront LOS channel with half-wavelength antenna spacings, $\theta_t = 0,$ $\theta_r = \pi/6,$ and $\phi = \pi/4:$ 1-bit beamforming (exact values in solid, interval spanned by the bounds in shaded) vs equiprobable signaling. Also shown is the performance with full resolution.

point that has been verified by contrasting the asymptotic performance of equiprobable signaling in a variety of such channels against the respective $C_\infty.$

B. LOS with Spherical Wavefronts

The scope of channels in this class is very large, depending on the array topologies and relative orientations; for the sake of specificity, we concentrate on ULAs, and draw insights whose generalization would be welcome follow-up work. A key property of ULA-spawned channels within this class is that [66]

$$\mathbf{H}^* \mathbf{H} \approx \frac{N_{\max}}{\eta} \mathbf{D}_{\text{tx}}^* \mathbf{F} \text{diag}(\underbrace{1, \dots, 1}_{\eta N_{\min}}, 0, \dots, 0) \mathbf{F}^* \mathbf{D}_{\text{tx}}$$

where the approximation sharpens with the numbers of antennas while \mathbf{F} is a unitary Fourier matrix, \mathbf{D}_{tx} and η

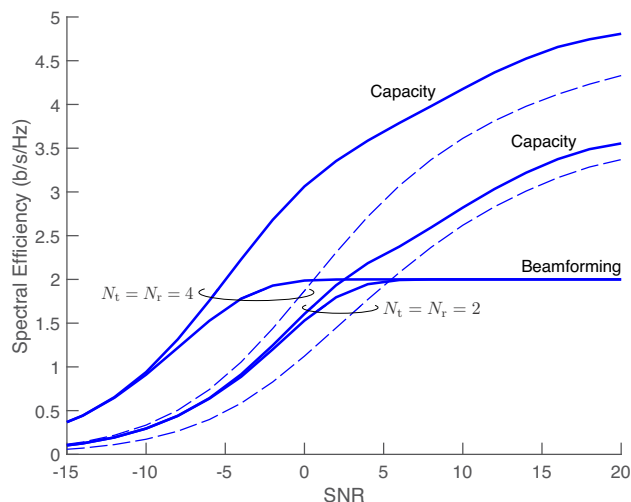


Fig. 5: Spectral efficiency as a function of SNR for $N_t = N_r = 2$ and $N_t = N_r = 4$, in a planar-wavefront LOS channel with half-wavelength antenna spacings, $\theta_t = \pi/4$, $\theta_r = \pi/6$, and $\phi = \pi/4$. In solid, capacity and beamforming; in dashed, equiprobable signaling.

are as introduced in Sec. II-B, and $N_{\min} = \min(N_t, N_r)$. Therefore, $\lambda_0 \approx N_{\max}/\eta$ and $\|\mathbf{v}_0\|_1^2 \approx N_t$.

By specializing (39), the optimum $\frac{E_b}{N_0 \min}$ attained by beamforming is seen to satisfy

$$\frac{\pi\eta}{2N_{\max} \log_2 e} \lesssim \frac{E_b}{N_0 \min} \lesssim \frac{\pi^3\eta}{16N_{\max} \log_2 e}, \quad (46)$$

which indicates that a smaller η is preferable at low SNR, meaning antennas as tightly spaced as possible—this renders the wavefronts maximally planar—and array orientations as endfire as possible—this shrinks their effective widths. Indeed, wavefront curvatures trim the beamforming gains, and reducing η mitigates the extent of such curvatures.

With growing η , the low-SNR performance does degrade, but beamforming retains an edge over equiprobable signaling for $\eta < 1$ or $N_t > N_r$. Alternatively, for $\eta = 1$ and $N_t = N_r$, (46) is no better than the equiprobable-signaling $\frac{E_b}{N_0 \min}$ in (40). In fact, for this all-important configuration whose eigenvalues are equal [67], [75]–[79], any transmission strategy achieves this same $\frac{E_b}{N_0 \min}$; this can be verified by using $\mathbf{H}^* \mathbf{H} = N_r \mathbf{I}$ and $\|\mathbf{x}_k\|_2^2 = 2N_t$ in (36), whereby (40) emerges irrespective of p_1, \dots, p_{4N_t-1} . This coincidence of $\frac{E_b}{N_0 \min}$ for all transmission strategies when $\eta = 1$ and $N_t = N_r$ does not translate to S_0 , which is decidedly larger for equiprobable signaling, indicating that this is the optimum low-SNR technique for this configuration as illustrated in Fig. 6. Precisely, applying (29) and (41), a channel with $\eta = 1$ and $N_t = N_r = N$ is seen to exhibit

$$S_0 = \frac{\frac{2}{\pi-1} N^4}{N^3 - \frac{2}{3} \sum_{n=0}^{N-1} \sum_{m=0}^{N-1} [\cos^4(2\pi \frac{nm}{N}) + \sin^4(2\pi \frac{nm}{N})]}. \quad (47)$$

Let us now turn to intermediate SNRs, where the full-resolution wisdom is that the performance depends only

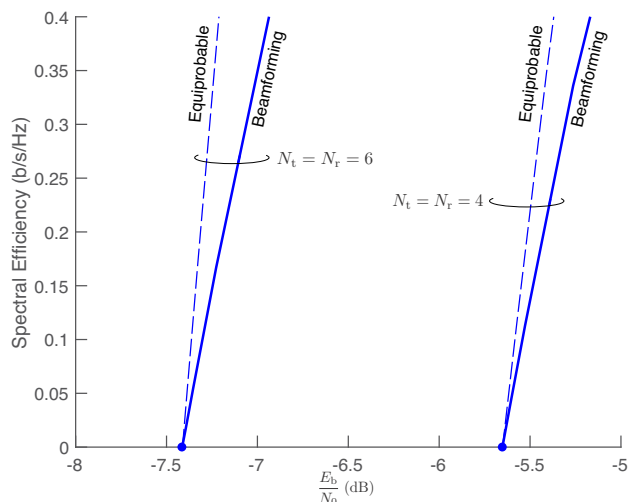


Fig. 6: Spectral efficiency as a function of E_b/N_0 for $N_t = N_r = 4$ and $N_t = N_r = 6$ in an LOS channel with $\eta = 1$. In solid, beamforming performance; in dashed, capacity with equiprobable signaling.

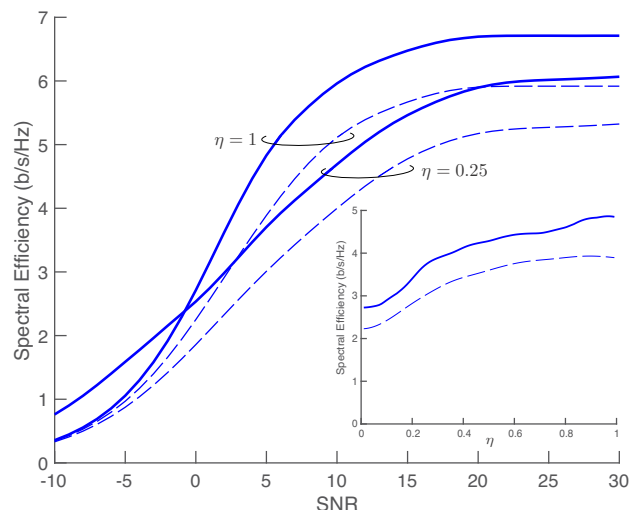


Fig. 7: Main plot: spectral efficiency as a function of SNR for $N_t = N_r = 4$, both with optimized (solid lines) and with uniform (dashed lines) quartet probabilities. Inset: spectral efficiency as a function of η for SNR = 5 dB. The channel is LOS and the arrays are broadside with $d_t = d_r$.

on η and it improves monotonically with η up to $\eta = 1$, where capacity is achieved by IID signaling. All these insights, underpinned by the approximate equality of the ηN_{\min} nonzero eigenvalues of $\mathbf{H}^* \mathbf{H}$, cease to hold in the 1-bit realm due to the transmitter's inability of accessing those singular values directly via precoding. Indeed, when the only ability is to manipulate the quartet probabilities (see Fig. 7 for an example):

- The performance does not depend only on η , but further on θ_t , θ_r , ϕ , D , and d_t and d_r .
- The optimum configuration need not correspond to $\eta = 1$.

The main takeaway for our purpose, though, is that at intermediate SNRs equiprobable signaling closely tracks the capacity.

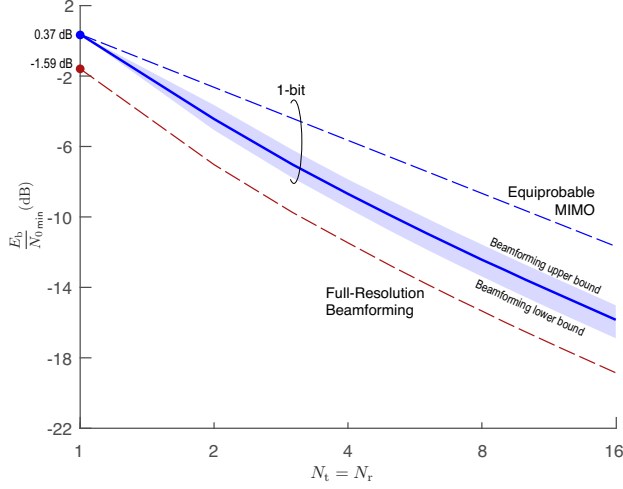


Fig. 8: Minimum $\frac{E_b}{N_0}$ vs $N_t = N_r$ for an IID Rayleigh-faded channel: 1-bit beamforming (exact values in solid, interval spanned by the bounds in shaded) vs equiprobable signaling. Also shown is the performance with full resolution.

C. IID Rayleigh Fading

For \mathbf{H} having IID complex Gaussian entries, we resort to the ergodic interpretation. Shown in Fig. 8 is the evolution of $\frac{E_b}{N_0 \min}$ with the number of antennas for the optimum strategy (beamforming on every channel realization) as well as for equiprobable signaling. The bounds in (39) provide an effective characterization of the optimum $\frac{E_b}{N_0 \min}$. Moreover, λ_0 and \mathbf{v}_0 are independent [80, lemma 5] and, although $\mathbb{E}[\lambda_0]$ does not lend itself to a general characterization, for growing N_t and N_r it approaches $(\sqrt{N_t} + \sqrt{N_r})^2$. Thus, beamforming achieves

$$\begin{aligned} \frac{\pi}{2(\sqrt{N_t} + \sqrt{N_r})^2 \log_2 e} &\lesssim \frac{E_b}{N_0 \min} \\ &\lesssim \frac{\pi^3 N_t}{16(\sqrt{N_t} + \sqrt{N_r})^2 \mathbb{E}[\|\mathbf{v}_0\|_1^2]} \end{aligned} \quad (48)$$

which sharpens with N_t and N_r . For $N_t = N_r = 64$, for instance, (48) gives $\frac{E_b}{N_0 \min} \in [-21.77, -23, 71]$ dB, correctly placing the actual value of -22.21 dB. The term $\mathbb{E}[\|\mathbf{v}_0\|_1^2]$ is readily computable for given values of N_t and we note, as a possible path to taming it analytically, that \mathbf{v}_0 is a column of a standard unitary matrix, uniformly distributed over an N_t -dimensional sphere.

With equiprobable signaling, $\frac{E_b}{N_0 \min}$ is given by (40) and we can further characterize S_0 . Starting from (29) and using

$$\begin{aligned} (\text{nondiag}(\mathbf{H}\mathbf{H}^*))^2 &= (\mathbf{H}\mathbf{H}^*)^2 - \mathbf{H}\mathbf{H}^* \text{diag}(\mathbf{H}\mathbf{H}^*) \\ &\quad - \text{diag}(\mathbf{H}\mathbf{H}^*) \mathbf{H}\mathbf{H}^* \\ &\quad + (\text{diag}(\mathbf{H}\mathbf{H}^*))^2 \end{aligned} \quad (49)$$

in conjunction with [80, lemma 4]

$$\mathbb{E}[\text{tr}((\mathbf{H}\mathbf{H}^*)^2)] = N_t N_r (N_t + N_r) \quad (50)$$

$$\mathbb{E}[\text{tr}(\mathbf{H}\mathbf{H}^* \text{diag}(\mathbf{H}\mathbf{H}^*))] = N_t N_t (N_t + 1) \quad (51)$$

$$\mathbb{E}[\text{tr}(\text{diag}(\mathbf{H}\mathbf{H}^*) \mathbf{H}\mathbf{H}^*)] = N_t N_t (N_t + 1) \quad (52)$$

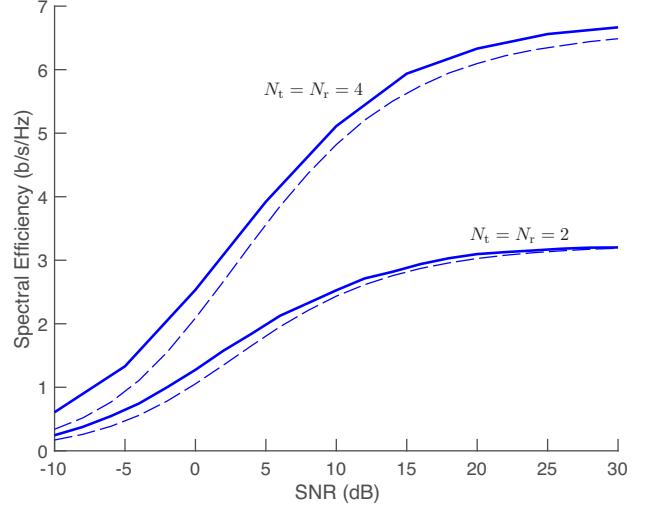


Fig. 9: Ergodic spectral efficiency vs SNR for $N_t = N_r = 2$ and 4 both with optimized (solid lines) and with equiprobable (dashed lines) signaling. The channel is IID Rayleigh-faded.

$$\mathbb{E}[\text{tr}((\text{diag}(\mathbf{H}\mathbf{H}^*))^2)] = N_t N_r (N_t + 1) \quad (53)$$

we have that

$$\mathbb{E}[\text{tr}((\text{nondiag}(\mathbf{H}\mathbf{H}^*))^2)] = N_t N_r (N_r - 1). \quad (54)$$

In turn,

$$\mathbb{E}[\|\mathbf{H}\mathbf{x}\|_4^4] = 6N_t^2 N_r \quad (55)$$

and, altogether,

$$S_0 = \frac{2N_t N_r}{(\pi - 1)N_t + N_r - 1}, \quad (56)$$

which is an increasing function of both N_t and N_r .

At intermediate SNRs, equiprobable signaling is remarkably effective (see Fig. 9). At the same time, the complexity of computing the mutual information—for equiprobable signaling, let alone with optimized quartet probabilities—is compounded by the need to expect it over the distribution of \mathbf{H} , to the point of becoming unwieldy even for very small antenna counts. Analytical characterizations are thus utterly necessary, and it is shown in Appendix B that

$$\begin{aligned} \mathbb{E}_{\mathbf{H}}[\mathcal{I}(\text{SNR}, \mathbf{H})] &= \mathbb{E}_{\mathbf{H}}[\mathcal{H}(\mathbf{y})] \\ &\quad - \frac{2N_r}{\sqrt{2\pi}} \int_{-\infty}^{\infty} \mathcal{H}_b(Q(-\sqrt{\text{SNR}}\xi)) e^{-\xi^2/2} d\xi \end{aligned} \quad (57)$$

with

$$\begin{aligned} 2N_r &\geq \mathbb{E}_{\mathbf{H}}[\mathcal{H}(\mathbf{y})] \geq 2N_t - 2N_r \\ &\quad - \log_2 \left[\sum_{i=0}^{N_t} \binom{N_t}{i}^2 \left(\frac{1}{4\pi^2} \arccos^2 \left(\frac{2i}{N_t} - 1 \right) \right)^{N_r} \right. \\ &\quad \left. + 2 \sum_{i=0}^{N_t} \sum_{j=i+1}^{N_t} \binom{N_t}{i} \binom{N_t}{j} P_{\cap}^{N_r}(i, j) \right] \end{aligned} \quad (58)$$

where $P_{\cap}(i, j)$ is given by (59).

The bounds specified by (57)–(59) are readily computable even for very large numbers of antennas. For

TABLE I: Lower bound on $\mathbb{E}_{\mathbf{H}}[\mathcal{H}(\mathbf{y})]$ as a function of N_t and N_r .

$N_r \downarrow N_t \rightarrow$	1	2	4	8	16	32
1	2	2	2	2	2	2
2	2	3.02	3.65	3.85	3.92	3.96
4	2	3.81	6.07	7.15	7.57	7.78
8	2	4	7.79	12.35	14.14	15.03
16	2	4	8	15.87	24.81	28.14
32	2	4	8	16	31.96	49.6

$N_t = N_r = 64$, for instance, a direct evaluation of $\mathbb{E}_{\mathbf{H}}[\mathcal{I}(\text{SNR}, \mathbf{H})]$ would require the $\mathcal{I}(\text{SNR}, \mathbf{H})$ for many realizations of \mathbf{H} , with each such mutual information calculation involving over 10^{75} terms. In contrast, the bounds entail the single SNR-dependent integral in (57) along with (58), which does not depend on the SNR and can be precomputed; Table I provides such precomputation for a range of antenna counts. Also of interest is that the upper bound becomes exact for $\text{SNR} \rightarrow 0$.

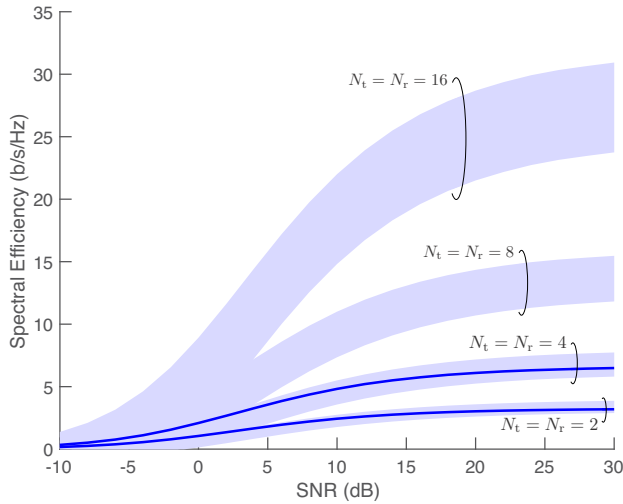


Fig. 10: Ergodic spectral efficiency as a function of SNR with equiprobable signaling: the shaded areas are the bounding regions, the solid lines are the actual values for $N_t = N_r = 2$ and $N_t = N_r = 4$. The channel is IID Rayleigh-faded.

The range specified by the bounds is illustrated in Fig. 10 for various values of $N_t = N_r$, alongside the actual spectral efficiencies (obtained via Monte-Carlo) for $N_t = N_r = 2$ and $N_t = N_r = 4$.

For $N_t > N_r$, the lower bound approaches its upper counterpart and, for $N_t \gg N_r$,

$$\mathbb{E}_{\mathbf{H}}[\mathcal{I}(\text{SNR}, \mathbf{H})] \approx 2N_r \left(1 - \frac{1}{\sqrt{2\pi}} \int_{-\infty}^{\infty} \mathcal{H}_b(Q(-\sqrt{\text{SNR}}\xi)) e^{-\xi^2/2} d\xi \right). \quad (60)$$

Indeed, as detailed in Appendix B, this approximation becomes an exact result for $N_r = 1$ or for $N_t \rightarrow \infty$ with N_r arbitrary.

$$P_{\cap}(i, j) = \frac{1}{2\pi} \int_0^{\infty} \int_0^{\infty} \operatorname{erfc} \left(-\frac{\gamma(N_t - i - j) + \xi(i - j)}{\sqrt{i(N_t - i) + j(N_t - j)}} \right) \operatorname{erfc} \left(\frac{\gamma(i - j) - \xi(N_t - i - j)}{\sqrt{i(N_t - i) + j(N_t - j)}} \right) e^{-2(\gamma^2 + \xi^2)} d\gamma d\xi \quad (59)$$

Some examples for $N_t = 4N_r$, presented in Fig. 11, confirm how precisely the ergodic spectral efficiency is determined when the antenna counts are somewhat skewed.

VIII. CONCLUSION

A host of issues that are thoroughly understood for full-resolution settings must be tackled anew for 1-bit MIMO communication. In particular, the computation of the capacity becomes unwieldy for even very modest dimensionalities and the derivation of general precoding solutions becomes a formidable task, itself power-consuming. Fortunately, in the single-user case such general precoding can be circumvented via a judicious switching between beamforming and equiprobable signaling, with the added benefits that these transmissions strategies are much more amenable to analytical characterizations and that their requirements in terms of channel-state information at the transmitter are minimal: $\log_2 4^{N_t-1} = 4(N_t - 1)$ bits for beamforming, none for equiprobable signaling.

The transition from beamforming to equiprobable signaling could be finessed by progressively activating quartets as the SNR grows, but the results in this paper suggest that there is a small margin of improvement: a direct switching at some appropriate point suffices to operate within a few dB of capacity at both low and intermediate SNRs. It would be of interest to gauge this shortfall for more intricate channel models such as those in [81]–[83].

Channel estimation at the receiver is an important aspect, with the need for procedures that avoid having to painstakingly gauge all the transition probabilities between \mathbf{x} and \mathbf{y} to deduce \mathbf{H} . Of much interest would be to extend existing results for channel estimation with full-resolution DACs and 1-bit ADCs [24], [25], [84]–[86] to the complete 1-bit realm. Equally pertinent would be to establish the bandwidths over which a frequency-flat representation suffices for each channel model, and to extend the respective analyses to account for intersymbol interference. This is acutely important given the impossibility of implementing OFDM with 1-bit converters.

In those multiuser settings where orthogonal (time/frequency) multiple access is effective, switching between beamforming and equiprobable signaling is also enticing. In other cases, chiefly if the antenna numbers are highly asymmetric, orthogonal multiple access is decidedly suboptimum, and there is room for more general schemes. We hope that the results in this paper can serve as a stepping stone to such schemes.

APPENDIX A

Let $\sigma_0, \dots, \sigma_{N_t-1}$ be the singular values of \mathbf{H} , ordered from largest to smallest, while \mathbf{u}_m and \mathbf{v}_m are the left

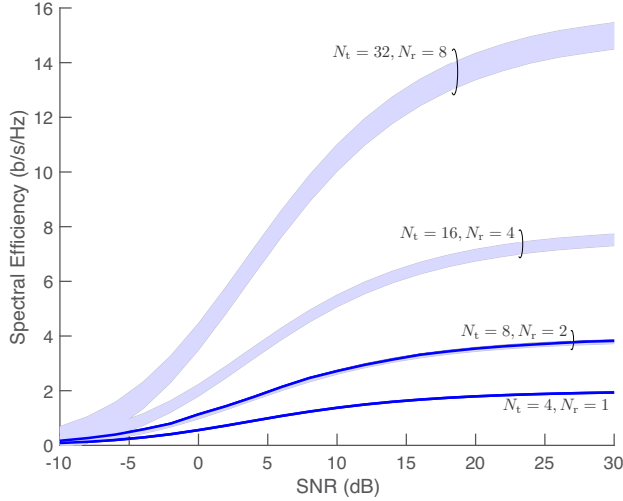


Fig. 11: Ergodic spectral efficiency as a function of SNR with equiprobable signaling: the shaded areas are the bounding regions, the solid lines are the actual values for $N_t = 4, N_r = 1$ and $N_t = 8, N_r = 2$. The channel is IID Rayleigh-faded.

and right singular vectors corresponding to σ_m . From the singular value decomposition

$$\mathbf{H} = \sum_{m=0}^{N_{\min}-1} \sigma_m \mathbf{u}_m \mathbf{v}_m^* \quad (61)$$

we have that

$$\|\mathbf{H}\mathbf{x}\|^2 = \sum_{m=0}^{N_{\min}-1} \sigma_m^2 |\mathbf{v}_m^* \mathbf{x}|^2, \quad (62)$$

which is the quantity to maximize. Under full-resolution transmission, (62) is maximized by $\mathbf{x} \propto \mathbf{v}_0$: complete projection on the dimension exhibiting the largest gain and zero projection elsewhere [72, sec. 5.3]. With 1-bit transmission, perfect alignment with \mathbf{v}_0 is generally not possible, and the goal becomes to determine which \mathbf{x} best aligns. If \mathbf{H} is rank-1, then such \mathbf{x} is sure to maximize (62). If the rank is plural, however, optimality cannot be guaranteed from best alignment with \mathbf{v}_0 because some other \mathbf{x} leaning further away could have a more favorable projection across the rest of dimensions. Suppose, for instance, that the rank is 3; if the \mathbf{x} best aligned with \mathbf{v}_0 does not further project on \mathbf{v}_1 , but only on \mathbf{v}_2 , there could be another \mathbf{x} aligning slightly less with \mathbf{v}_0 but projecting also on \mathbf{v}_1 in a way that yields a higher metric in (62). This possibility may arise when the largest singular value is not very dominant. Even then, though, the \mathbf{x} that projects maximally on \mathbf{v}_0 is bound to perform well.

Values of \mathbf{x} that align well with \mathbf{v}_0 can be obtained as $\mathbf{x} = \text{sgn}(e^{j\varphi} \mathbf{v}_0)$ where φ allows setting the absolute phase arbitrarily before quantization. Letting φ run from 0 to 2π , every entry of the quantized \mathbf{x} changes four times and a subset of $4N_t$ vectors \mathbf{x} is obtained. These $4N_t$ vectors actually belong to N_t quartets because, if \mathbf{x}_k is in the k th subset, $j\mathbf{x}_k$ is sure to be there too. Since identifying one representative per quartet suffices for our purposes, attention can be restricted to those values of φ

that trigger a change in $\text{sgn}(e^{j\varphi} \mathbf{v}_0)$, i.e., $\varphi = \angle(v_{0,m})$ for $m = 0, \dots, N_t - 1$. Letting $\varphi_m = \angle(v_{0,m}) + \epsilon$ with ϵ a small quantity, we obtain the subset of N_t quartet representatives as

$$\mathbf{x}_k = \text{sgn}(e^{j\varphi_{k-1}} \mathbf{v}_0) \quad k = 1, \dots, N_t. \quad (63)$$

The sign of ϵ is irrelevant, it merely changes which representative is selected for each quartet. Confirming the intuition that the N_t quartets in (63) are good choices, it is proved in [47] that the quartet that best aligns with \mathbf{v}_0 is sure to be in this subset. Thus, searching a subset of N_t candidates suffices to beamform optimally in rank-1 channels, and quasi-optimally in higher-rank channels, without having to search the entire field of 4^{N_t-1} possibilities.

Let us now turn to the performance. An upper bound on $\|\mathbf{H}\mathbf{x}_{k^*}\|^2$ can be obtained by assuming that, on every channel realization, there is a value of \mathbf{x} that aligns perfectly with \mathbf{v}_0 . From (62), this gives

$$\|\mathbf{H}\mathbf{x}\|^2 \leq 2N_t \sigma_0^2, \quad (64)$$

which, along with (36), yields the lower bound in (39).

In turn, a lower bound on $\|\mathbf{H}\mathbf{x}_{k^*}\|^2$ is obtained for any choice of \mathbf{x} , and in particular for $\mathbf{x} = \text{sgn}(e^{j\varphi} \mathbf{v}_0)$ with $\varphi \in [-\pi/4, \pi/4]$, such that [47]

$$|\mathbf{v}_0^* \mathbf{x}_{k^*}| \geq \max_{\varphi \in [-\pi/4, \pi/4]} |\mathbf{v}_0^* \text{sgn}(e^{j\varphi} \mathbf{v}_0)| \quad (65)$$

$$\geq \mathbb{E}_{\varphi} [|\mathbf{v}_0^* \text{sgn}(e^{j\varphi} \mathbf{v}_0)|] \quad (66)$$

$$= \mathbb{E}_{\varphi} \left[\left| \sum_{m=0}^{N_t-1} v_{0,m}^* \text{sgn}(e^{j\varphi} v_{0,m}) \right| \right] \quad (67)$$

$$= \mathbb{E}_{\varphi} \left[\left| \sum_{m=0}^{N_t-1} |v_{0,m}| e^{-j\phi_m} \text{sgn}(e^{j(\varphi+\phi_m)}) \right| \right]$$

$$= \mathbb{E}_{\varphi} \left[\left| \sum_{m=0}^{N_t-1} |v_{0,m}| e^{j\varphi} e^{-j(\varphi+\phi_m)} \text{sgn}(e^{j(\varphi+\phi_m)}) \right| \right]$$

$$= \mathbb{E}_{\varphi} \left[\left| \sum_{m=0}^{N_t-1} |v_{0,m}| e^{-j(\varphi+\phi_m)} \text{sgn}(e^{j(\varphi+\phi_m)}) \right| \right].$$

For any $\theta \in [0, 2\pi]$, the phase of $e^{-j\theta} \text{sgn}(e^{j\theta})$ is within $[-\pi/4, \pi/4]$ while $|e^{-j\theta} \text{sgn}(e^{j\theta})| = \sqrt{2}$. Hence, letting $\theta_m = \varphi + \phi_m$,

$$|\mathbf{v}_0^* \mathbf{x}_{k^*}| \geq \sqrt{2} \mathbb{E}_{\theta_0, \dots, \theta_{N_t-1}} \left[\left| \sum_{m=0}^{N_t-1} |v_{0,m}| e^{-j\theta_m} \right| \right] \quad (68)$$

$$\geq \sqrt{2} \mathbb{E}_{\theta_0, \dots, \theta_{N_t-1}} \left[\left| \sum_{m=0}^{N_t-1} |v_{0,m}| \cos(\theta_m) \right| \right] \quad (69)$$

$$= \sqrt{2} \sum_{m=0}^{N_t-1} |v_{0,m}| \mathbb{E}[\cos(\theta_m)] \quad (70)$$

$$= \sqrt{2} \sum_{m=0}^{N_t-1} |v_{0,m}| \frac{2}{\pi} \int_{-\pi/4}^{\pi/4} \cos(\xi) d\xi \quad (71)$$

$$= \frac{4}{\pi} \sum_{m=0}^{N_t-1} |v_{0,m}| \quad (72)$$

$$= \frac{4}{\pi} \|\mathbf{v}_0\|_1, \quad (73)$$

where (70) holds because $\cos(\theta_m) > 0$ for $\theta_m \in [-\pi/4, \pi/4]$. Disregarding $|\mathbf{v}_m^* \mathbf{x}_{k^*}|$ for $m > 0$ in (62),

$$\|\mathbf{H} \mathbf{x}_{k^*}\|^2 \geq \frac{16}{\pi^2} \sigma_0^2 \|\mathbf{v}_0\|_1^2, \quad (74)$$

which, along with (36), yields the upper bound in (39).

APPENDIX B

In (23), for every n and k , $\Re\{\mathbf{h}_n \mathbf{x}_k\} \sim \mathcal{N}(0, N_t)$ and $\Im\{\mathbf{h}_n \mathbf{x}_k\} \sim \mathcal{N}(0, N_t)$. Thus, letting $r \sim \mathcal{N}(0, 1)$,

$$\begin{aligned} \mathbb{E}_{\mathbf{H}}[\mathcal{H}(\mathbf{y}|\mathbf{x})] &= 2N_r \mathbb{E}_r \left[\mathcal{H}_b \left(Q \left(-\sqrt{\text{SNR}} r \right) \right) \right] \\ &= \frac{2N_r}{\sqrt{2\pi}} \int_{-\infty}^{\infty} \mathcal{H}_b \left(Q \left(-\sqrt{\text{SNR}} \xi \right) \right) e^{-\xi^2/2} d\xi. \end{aligned} \quad (75)$$

In turn,

$$\mathbb{E}_{\mathbf{H}}[\mathcal{H}(\mathbf{y})] \leq 2N_r \quad (76)$$

with equality for $\text{SNR} \rightarrow 0$, when the receiver observes only noise and \mathbf{y} is equiprobably binary on $2N_r$ real dimensions. As the removal of noise can only decrease it, $\mathcal{H}(\mathbf{y})$ diminishes as the SNR grows, being lower-bounded by its value for $\text{SNR} \rightarrow \infty$. The expectation of such noiseless lower bound over \mathbf{H} can be elaborated by generalizing to our complex setting a clever derivation in [46], starting from

$$\begin{aligned} \mathbb{E}_{\mathbf{H}}[\mathcal{H}(\mathbf{y})] &= \mathbb{E}_{\mathbf{H}} \left[\sum_{\ell=1}^{4N_r} p_{\mathbf{y}}(\mathbf{y}_{\ell}) \log_2 \frac{1}{p_{\mathbf{y}}(\mathbf{y}_{\ell})} \right] \\ &= \mathbb{E}_{\mathbf{H}} \left[\sum_{\ell=1}^{4N_r} \mathbb{E}_{\mathbf{x}} [p_{\mathbf{y}|\mathbf{x}}(\mathbf{y}_{\ell}|\mathbf{x})] \log_2 \frac{1}{\mathbb{E}_{\mathbf{x}} [p_{\mathbf{y}|\mathbf{x}}(\mathbf{y}_{\ell}|\mathbf{x})]} \right] \\ &= \mathbb{E}_{\mathbf{H}} \left[\sum_{\ell=1}^{4N_r} \mathbb{E}_{\mathbf{x}} [1\{\text{sgn}(\mathbf{H}\mathbf{x}) = \mathbf{y}_{\ell}\}] \right. \\ &\quad \left. \cdot \log_2 \frac{1}{\mathbb{E}_{\mathbf{x}} [1\{\text{sgn}(\mathbf{H}\mathbf{x}) = \mathbf{y}_{\ell}\}]} \right] \end{aligned} \quad (78)$$

where $1\{\cdot\}$ is the indicator function. Since \mathbf{H} is isotropic and \mathbf{x} is equiprobable, no \mathbf{y}_{ℓ} is favored over the rest in terms of the probability of $\text{sgn}(\mathbf{H}\mathbf{x})$ equalling such \mathbf{y}_{ℓ} . Hence, (78) can be evaluated for any specific \mathbf{y}_{ℓ} , say \mathbf{y}_1 whose entries all equal $1 + j$. This gives

$$\begin{aligned} \mathbb{E}_{\mathbf{H}}[\mathcal{H}(\mathbf{y})] &= 4^{N_r} \mathbb{E}_{\mathbf{H}} \left[\mathbb{E}_{\mathbf{x}} [1\{\text{sgn}(\mathbf{H}\mathbf{x}) = \mathbf{y}_1\}] \right. \\ &\quad \left. \cdot \log_2 \frac{1}{\mathbb{E}_{\mathbf{x}} [1\{\text{sgn}(\mathbf{H}\mathbf{x}) = \mathbf{y}_1\}]} \right]. \end{aligned} \quad (79)$$

Likewise, the probability that $\text{sgn}(\mathbf{H}\mathbf{x}) = \mathbf{y}_1$ is common to every realization of \mathbf{x} and thus

$$\begin{aligned} \mathbb{E}_{\mathbf{H}}[\mathcal{H}(\mathbf{y})] &= -4^{N_r} \mathbb{E}_{\mathbf{H}} [1\{\text{sgn}(\mathbf{H}\mathbf{x}_1) = \mathbf{y}_1\}] \\ &\quad \cdot \log_2 \mathbb{E}_{\mathbf{x}} [1\{\text{sgn}(\mathbf{H}\mathbf{x}) = \mathbf{y}_1\}] \end{aligned} \quad (80)$$

where all entries of \mathbf{x}_1 equal $1 + j$ and where it is convenient to retain the second expectation over \mathbf{x} in order to later solve its counterpart over \mathbf{H} . Then,

$$\begin{aligned} \mathbb{E}_{\mathbf{H}}[\mathcal{H}(\mathbf{y})] &= -4^{N_r} \mathbb{E}_{\mathbf{H}|\text{sgn}(\mathbf{H}\mathbf{x}_1)=\mathbf{y}_1} [1\{\text{sgn}(\mathbf{H}\mathbf{x}_1) = \mathbf{y}_1\}] \\ &\quad \cdot \log_2 \mathbb{E}_{\mathbf{x}} [1\{\text{sgn}(\mathbf{H}\mathbf{x}) = \mathbf{y}_1\}] \\ &\quad \cdot \mathbb{P}[\text{sgn}(\mathbf{H}\mathbf{x}_1) = \mathbf{y}_1] \end{aligned} \quad (81)$$

and, since $\mathbb{P}[\text{sgn}(\mathbf{H}\mathbf{x}_1) = \mathbf{y}_1] = \frac{1}{4^{N_r}}$ and the factor $1\{\text{sgn}(\mathbf{H}\mathbf{x}_1) = \mathbf{y}_1\}$ becomes immaterial once the expectation over \mathbf{H} has been conditioned on $\text{sgn}(\mathbf{H}\mathbf{x}_1)$,

$$\begin{aligned} \mathbb{E}_{\mathbf{H}}[\mathcal{H}(\mathbf{y})] &= -\mathbb{E}_{\mathbf{H}|\text{sgn}(\mathbf{H}\mathbf{x}_1)=\mathbf{y}_1} \left[\log_2 \mathbb{E}_{\mathbf{x}} [1\{\text{sgn}(\mathbf{H}\mathbf{x}) = \mathbf{y}_1\}] \right] \\ &= -\mathbb{E}_{\mathbf{H}|\text{sgn}(\mathbf{H}\mathbf{x}_1)=\mathbf{y}_1} \left[\log_2 \frac{1}{4^{N_t}} \sum_{k=1}^{4N_t} 1\{\text{sgn}(\mathbf{H}\mathbf{x}_k) = \mathbf{y}_1\} \right] \\ &= 2N_t - \mathbb{E}_{\mathbf{H}|\text{sgn}(\mathbf{H}\mathbf{x}_1)=\mathbf{y}_1} \left[\log_2 \sum_{k=1}^{4N_t} 1\{\text{sgn}(\mathbf{H}\mathbf{x}_k) = \mathbf{y}_1\} \right] \\ &\geq 2N_t - \log_2 \sum_{k=1}^{4N_t} \mathbb{E}_{\mathbf{H}|\text{sgn}(\mathbf{H}\mathbf{x}_1)=\mathbf{y}_1} [1\{\text{sgn}(\mathbf{H}\mathbf{x}_k) = \mathbf{y}_1\}] \end{aligned} \quad (82)$$

where the last step follows from Jensen's inequality. Since the expectation of an indicator function yields the probability of the underlying event,

$$\begin{aligned} \mathbb{E}_{\mathbf{H}}[\mathcal{H}(\mathbf{y})] &\geq 2N_t \\ &\quad - \log_2 \sum_{k=1}^{4N_t} \mathbb{P}[\text{sgn}(\mathbf{H}\mathbf{x}_k) = \mathbf{y}_1 | \text{sgn}(\mathbf{H}\mathbf{x}_1) = \mathbf{y}_1] \end{aligned} \quad (83)$$

with

$$\begin{aligned} \mathbb{P}[\text{sgn}(\mathbf{H}\mathbf{x}_k) = \mathbf{y}_1 | \text{sgn}(\mathbf{H}\mathbf{x}_1) = \mathbf{y}_1] &= \frac{\mathbb{P}[\text{sgn}(\mathbf{H}\mathbf{x}_k) = \mathbf{y}_1 \cap \text{sgn}(\mathbf{H}\mathbf{x}_1) = \mathbf{y}_1]}{\mathbb{P}[\text{sgn}(\mathbf{H}\mathbf{x}_1) = \mathbf{y}_1]} \\ &= 4^{N_r} \mathbb{P}[\text{sgn}(\mathbf{H}\mathbf{x}_k) = \mathbf{y}_1 \cap \text{sgn}(\mathbf{H}\mathbf{x}_1) = \mathbf{y}_1]. \end{aligned} \quad (84)$$

As the channel has IID entries, letting \mathbf{h} be an arbitrary row of \mathbf{H} ,

$$\mathbb{P}[\text{sgn}(\mathbf{H}\mathbf{x}_k) = \mathbf{y}_1 \cap \text{sgn}(\mathbf{H}\mathbf{x}_1) = \mathbf{y}_1] = (P_{\cap})^{N_r} \quad (85)$$

with

$$\begin{aligned} P_{\cap} &= \mathbb{P}[\text{sgn}(\mathbf{h}\mathbf{x}_k) = (1 + j) \cap \text{sgn}(\mathbf{h}\mathbf{x}_1) = (1 + j)] \\ &= \mathbb{P}[\text{sgn}(\Re\{\mathbf{h}\mathbf{x}_k\}) = 1 \cap \text{sgn}(\Im\{\mathbf{h}\mathbf{x}_k\}) = 1 \\ &\quad \cap \text{sgn}(\Re\{\mathbf{h}\mathbf{x}_1\}) = 1 \cap \text{sgn}(\Im\{\mathbf{h}\mathbf{x}_1\}) = 1] \\ &= \mathbb{P}[\Re\{\mathbf{h}\mathbf{x}_k\} > 0 \cap \Im\{\mathbf{h}\mathbf{x}_k\} > 0 \\ &\quad \cap \Re\{\mathbf{h}\mathbf{x}_1\} > 0 \cap \Im\{\mathbf{h}\mathbf{x}_1\} > 0]. \end{aligned} \quad (86)$$

Defining $a_k = \mathbf{h}\mathbf{x}_k$ and $a_1 = \mathbf{h}\mathbf{x}_1$,

$$\begin{aligned} P_{\cap} &= \int_0^{\infty} \int_0^{\infty} \int_0^{\infty} \int_0^{\infty} f_{\Re\{a_k\}\Im\{a_k\}\Re\{a_1\}\Im\{a_1\}}(\alpha, \beta, \gamma, \xi) \\ &\quad \cdot d\alpha d\beta d\gamma d\xi \end{aligned} \quad (88)$$

$$f_{\Re\{a_k\}\Im\{a_k\}\Re\{a_1\}\Im\{a_1\}}(\alpha, \beta, \gamma, \xi) = \frac{1}{8\pi^2} \frac{1}{i(N_t - i) + j(N_t - j)} \exp\left(-\frac{1}{4} \frac{[\alpha \ \beta \ \gamma \ \xi] \Sigma_k^{-1} [\alpha \ \beta \ \gamma \ \xi]^T}{i(N_t - i) + j(N_t - j)}\right) \quad (93)$$

with $\Re\{a_k\}$, $\Im\{a_k\}$, $\Re\{a_1\}$, and $\Im\{a_1\}$ jointly Gaussian with mean zero and covariance

$$\Sigma_k = \begin{bmatrix} N_t \mathbf{I} & \mathbf{R}_k \\ \mathbf{R}_k & N_t \mathbf{I} \end{bmatrix} \quad (89)$$

where \mathbf{I} is the 2×2 identity matrix while

$$\mathbf{R}_k = \begin{bmatrix} N_t - i - j & j - i \\ i - j & N_t - i - j \end{bmatrix}. \quad (90)$$

with i and j the respective number of entries of $\Re\{a_k\}$ and $\Im\{a_k\}$ that are -1 , the rest of their entries (along with all the entries of $\Re\{a_1\}$ and $\Im\{a_1\}$) being $+1$. Most importantly, because the entries of \mathbf{h} are IID, the position of those -1 values is immaterial and only their totals i and j matter. Altogether, the joint distribution of $\Re\{a_k\}$, $\Im\{a_k\}$, $\Re\{a_1\}$ and $\Im\{a_1\}$ is as in (93) and, plugging it in (88) and tediously integrating over two of the dimensions, what emerges is (59) with the dependence on i and j made explicit and with $\text{erfc}(\cdot)$ the complementary error function.

Returning to (83), and accounting for the number of indices k that map to each i and j ,

$$\begin{aligned} \mathbb{E}_{\mathbf{H}}[\mathcal{H}(\mathbf{y})] &\geq 2N_t - 2N_r \\ &- \log_2 \sum_{i=0}^{N_t} \sum_{j=0}^{N_t} \binom{N_t}{i} \binom{N_t}{j} P_{\cap}^{N_r}(i, j). \end{aligned} \quad (91)$$

For $i = j$, (59) can be integrated into

$$P_{\cap}(i, i) = \frac{1}{4\pi^2} \arccos\left(\frac{2i}{N_t} - 1\right) \quad (92)$$

with $P_{\cap}(0, 0) = 1/4$ and $P_{\cap}(N_t, N_t) = 0$. Furthermore, $P_{\cap}(i, j) = P_{\cap}(j, i)$ with $P_{\cap}(0, N_t) = P_{\cap}(N_t, 0) = 0$. With these relationships accounted for, (91) yields (58).

Let us now consider some special cases of interest. For $N_t = 1$, (58) reduces to

$$\mathbb{E}_{\mathbf{H}}[\mathcal{H}(\mathbf{y})] \geq 2 - 2N_r - \log_2(4^{-N_r} + 4P_{\cap}(0, 1)) \quad (94)$$

and, since $P_{\cap}(0, 1) = 0$, further to $\mathbb{E}_{\mathbf{H}}[\mathcal{H}(\mathbf{y})] \geq 2$. In fact, in this case $\mathcal{H}(\mathbf{y}) = 2$ for every channel realization and thus $\mathbb{E}_{\mathbf{H}}[\mathcal{H}(\mathbf{y})] = 2$.

For $N_r = 1$, the scalar quantized signal y takes four equiprobable values—again, not only on average, but for every channel realization—and thus $\mathbb{E}_{\mathbf{H}}[\mathcal{H}(\mathbf{y})] = 2$.

For fixed N_t and $N_r \rightarrow \infty$, the key is the observation that $P_{\cap}(i, j)$ achieves its largest value for $i = j = 0$, namely $P_{\cap}(0, 0) = 1/4$. For $i > 0$ and/or $j > 0$, $P_{\cap}(i, j) < 1/4$ because any negative sign in either the real and imaginary parts of \mathbf{x}_k reduces the probability in (87). The largest term in the summations within the logarithm in (58) equals 4^{-N_r} and, as $N_r \rightarrow \infty$, every other term vanishes faster and the lower bound on $\mathbb{E}_{\mathbf{H}}[\mathcal{H}(\mathbf{y})]$ converges towards $2N_t$.

Finally, for fixed N_r and $N_t \rightarrow \infty$, the rows of \mathbf{H} become asymptotically orthogonal [72, sec. 5.4.2] and hence, for every realization of \mathbf{H} , \mathbf{y} consists of IID complex components. Again, $\mathbb{E}_{\mathbf{H}}[\mathcal{H}(\mathbf{y})] = 2N_r$.

For $N_r = 1$ and for $N_t \rightarrow \infty$ with fixed N_r , the above observations reveal that the lower and upper bounds coincide, fully determining, as per (60), the ergodic spectral efficiency with equiprobable signaling and IID Rayleigh fading.

REFERENCES

- [1] A. Lozano, "1-bit MIMO for terahertz channels," in *ITG Workshop on Smart Antennas (WSA)*, 2021.
- [2] R. Piesiewicz, T. Kleine-Ostmann, N. Krumbholz, D. Mittleman, M. Koch, J. Schoebel, and T. Kurner, "Short-range ultra-broadband terahertz communications: Concepts and perspectives," *IEEE Ant. and Prop. Magazine*, vol. 49, no. 6, pp. 24–39, 2007.
- [3] I. F. Akyildiz, J. Jornet, and C. Han, "Terahertz band: Next frontier for wireless communications," *Physical Commun.*, vol. 12, pp. 16–32, 2014.
- [4] H. Elayan, O. Amin, B. Shihada, R. Shubair, and M.-S. Alouini, "Terahertz band: The last piece of RF spectrum puzzle for communication systems," *IEEE Open J. Commun. Society*, vol. 1, pp. 1–32, 2019.
- [5] T. Rappaport, Y. Xing, O. Kanhere, S. Ju, A. Madanayake, S. Mandal, A. Alkhateeb, and G. Trichopoulos, "Wireless communications and applications above 100 GHz: Opportunities and challenges for 6G and beyond," *IEEE Access*, vol. 7, pp. 78729–78757, 2019.
- [6] A. Faisal, H. Sarrideen, H. Dahrouj, T. Y. Al-Naffouri, and M.-S. Alouini, "Ultramassive MIMO systems at terahertz bands: Prospects and challenges," *IEEE Veh. Techn. Magazine*, vol. 15, no. 4, pp. 33–42, 2020.
- [7] H.-S. Lee and C. G. Sodini, "Analog-to-digital converters: Digitizing the analog world," *Proc. IEEE*, vol. 96, no. 2, pp. 323–334, 2008.
- [8] B. Murmann, "The race for the extra decibel: A brief review of current ADC performance trajectories," *IEEE Solid-State Circuits Magazine*, vol. 7, no. 3, pp. 58–66, 2015.
- [9] P. Skrimponis, S. Dutta, M. Mezzavilla, S. Rangan, S. Mirfarshbafan, C. Studer, J. Buckwalter, and M. Rodwell, "Power consumption analysis for mobile mmWave and sub-THz receivers," in *6G Wireless Summit (6G SUMMIT)*, 2020.
- [10] I. D. O'Donnell and R. W. Brodersen, "An ultra-wideband transceiver architecture for low power, low rate, wireless systems," *IEEE Trans. Veh. Techn.*, vol. 54, no. 5, pp. 1623–1631, 2005.
- [11] B. Nasri, S. Sebastian, K. You, R. RanjithKumar, and D. Shahrjerdi, "A 700 μw 1GS/s 4-bit folding-flash ADC in 65nm CMOS for wideband wireless communications," in *IEEE Int'l Symp. Circuits and Systems (ISCAS)*, 2017.
- [12] E. Olieman, A.-J. Annema, and B. Nauta, "An interleaved full Nyquist high-speed DAC technique," *IEEE J. Solid-State Circuits*, vol. 50, no. 3, pp. 704–713, 2015.
- [13] Juanda, W. Shu, and J. Chang, "A calibration-free/DEM-free 8-bit 2.4-GS/s single-core digital-to-analog converter with a distributed biasing scheme," *IEEE Trans. VLSI Systems*, vol. 26, no. 11, pp. 2299–2309, 2018.
- [14] E. De Carvalho, A. Ali, A. Amiri, M. Angelichinoski, and R. W. Heath, "Non-stationarities in extra-large-scale massive MIMO," *IEEE Wireless Commun.*, vol. 27, no. 4, pp. 74–80, 2020.
- [15] J. A. Nossek and M. T. Ivrlač, "Capacity and coding for quantized MIMO systems," in *Int'l Conf. Wireless Commun. and Mobile Computing*, 2006, pp. 1387–1392.
- [16] A. Mezghani, M.-S. Khoufi, and J. A. Nossek, "A modified MMSE receiver for quantized MIMO systems," *Proc. ITG/IEEE WSA*, 2007.

- [17] A. Mezghani and J. A. Nossek, "Analysis of Rayleigh-fading channels with 1-bit quantized output," in *IEEE Int'l Symp. Inform. Theory (ISIT)*, 2008, pp. 260–264.
- [18] J. Singh, O. Dabeer, and U. Madhow, "On the limits of communication with low-precision analog-to-digital conversion at the receiver," *IEEE Trans. Commun.*, vol. 57, no. 12, pp. 3629–3639, 2009.
- [19] J. Singh, S. Ponnuru, and U. Madhow, "Multi-gigabit communication: The ADC bottleneck," in *IEEE Int'l Conf. Ubiquitous Wireless Broadband (ICUWB)*, 2009, pp. 22–27.
- [20] C. Studer and G. Durisi, "Quantized massive MU-MIMO-OFDM uplink," *IEEE Trans. Commun.*, vol. 64, no. 6, pp. 2387–2399, 2016.
- [21] L. Fan, S. Jin, C. Wen, and H. Zhang, "Uplink achievable rate for massive MIMO systems with low-resolution ADC," *IEEE Commun. Letters*, vol. 19, no. 12, pp. 2186–2189, 2015.
- [22] S. Wang, Y. Li, and J. Wang, "Multiuser detection in massive spatial modulation MIMO with low-resolution ADCs," *IEEE Trans. Wireless Commun.*, vol. 14, no. 4, pp. 2156–2168, 2014.
- [23] J. Mo and R. W. Heath, "Capacity analysis of one-bit quantized MIMO systems with transmitter channel state information," *IEEE Trans. Signal Processing*, vol. 63, no. 20, pp. 5498–5512, 2015.
- [24] C. Mollén, J. Choi, E. Larsson, and R. W. Heath, "Uplink performance of wideband massive MIMO with one-bit ADCs," *IEEE Trans. Wireless Commun.*, vol. 16, no. 1, pp. 87–100, 2017.
- [25] Y. Li, C. Tao, G. Seco-Granados, A. Mezghani, L. Swindlehurst, and L. Liu, "Channel estimation and performance analysis of one-bit massive MIMO systems," *IEEE Trans. Signal Processing*, vol. 65, no. 15, pp. 4075–4089, 2017.
- [26] S. Jacobsson, G. Durisi, M. Coldrey, U. Gustavsson, and C. Studer, "Throughput analysis of massive MIMO uplink with low-resolution ADCs," *IEEE Trans. Wireless Commun.*, vol. 16, no. 6, pp. 4038–4051, 2017.
- [27] B. Rassouli, M. Varasteh, and D. Gündüz, "Gaussian multiple access channels with one-bit quantizer at the receiver," *Entropy*, vol. 20, no. 9, p. 686, 2018.
- [28] A. Khalili, S. Rini, L. Barletta, E. Erkip, and Y. C. Eldar, "On MIMO channel capacity with output quantization constraints," in *IEEE Int'l Symp. Inform. Theory (ISIT)*, 2018, pp. 1355–1359.
- [29] A. Mezghani, J. A. Nossek, and A. L. Swindlehurst, "Low SNR asymptotic rates of vector channels with one-bit outputs," *IEEE Trans. Inform. Theory*, vol. 66, no. 12, pp. 7615–7634, 2020.
- [30] S. Jacobsson, G. Durisi, M. Coldrey, T. Goldstein, and C. Studer, "Nonlinear 1-bit precoding for massive MU-MIMO with higher-order modulation," in *Asilomar Conf. on Signals, Systems and Computers*, 2016, pp. 763–767.
- [31] A. Mezghani and J. A. Nossek, "On ultra-wideband MIMO systems with 1-bit quantized outputs: Performance analysis and input optimization," in *IEEE Int'l Symp. Inform. Theory (ISIT)*, 2007, pp. 1286–1289.
- [32] —, "Capacity lower bound of MIMO channels with output quantization and correlated noise," in *IEEE Int'l Symp. Inform. Theory (ISIT)*, 2012.
- [33] G.-J. Park and S.-N. Hong, "Construction of 1-bit transmit-signal vectors for downlink MU-MISO systems with PSK signaling," *IEEE Trans. Veh. Techn.*, vol. 68, no. 8, pp. 8270–8274, 2019.
- [34] H. Jedda, A. Mezghani, A. L. Swindlehurst, and J. A. Nossek, "Quantized constant envelope precoding with PSK and QAM signaling," *IEEE Trans. Wireless Communications*, vol. 17, no. 12, pp. 8022–8034, 2018.
- [35] M. Shao, Q. Li, W.-K. Ma, and A. So, "A framework for one-bit and constant-envelope precoding over multiuser massive MISO channels," *IEEE Trans. Signal Proc.*, vol. 67, no. 20, pp. 5309–5324, 2019.
- [36] F. Sahrabi, Y.-F. Liu, and W. Yu, "One-bit precoding and constellation range design for massive MIMO with QAM signaling," *IEEE J. Sel. Topics Signal Proc.*, vol. 12, no. 3, pp. 557–570, 2018.
- [37] O. Castañeda, S. Jacobsson, G. Durisi, M. Coldrey, T. Goldstein, and C. Studer, "1-bit massive MU-MIMO precoding in VLSI," *IEEE J. Emerging and Sel. Topics in Circuits and Systems*, vol. 7, no. 4, pp. 508–522, 2017.
- [38] O. Usman, H. Jedda, A. Mezghani, and J. Nossek, "MMSE precoder for massive MIMO using 1-bit quantization," in *IEEE Int'l Conf. Acoustics, Speech and Signal Processing (ICASSP)*, 2016.
- [39] A. Li, C. Masouros, F. Liu, and A. L. Swindlehurst, "Massive MIMO 1-bit DAC transmission: A low-complexity symbol scaling approach," *IEEE Trans. Wireless Commun.*, vol. 17, no. 11, pp. 7559–7575, 2018.
- [40] L. T. N. Landau and R. C. de Lamare, "Branch-and-bound precoding for multiuser MIMO systems with 1-bit quantization," *IEEE Wireless Commun. Letters*, vol. 6, no. 6, pp. 770–773, 2017.
- [41] G. Zeitler, A. C. Singer, and G. Kramer, "Low-precision A/D conversion for maximum information rate in channels with memory," *IEEE Trans. Commun.*, vol. 60, no. 9, pp. 2511–2521, 2012.
- [42] B. M. Murray and I. B. Collings, "AGC and quantization effects in a zero-forcing MIMO wireless system," in *IEEE Veh. Techn. Conf. (VTC)*, 2006.
- [43] T. Koch and A. Lapidoto, "At low SNR, asymmetric quantizers are better," *IEEE Trans. Inform. Theory*, vol. 59, no. 9, pp. 5421–5445, 2013.
- [44] J. Mo, A. Alkhateeb, S. Abu-Surra, and R. W. Heath, "Hybrid architectures with few-bit ADC receivers: Achievable rates and energy-rate tradeoffs," *IEEE Trans. Wireless Commun.*, vol. 16, no. 4, pp. 2274–2287, 2017.
- [45] N. Liang and W. Zhang, "Mixed-ADC massive MIMO," *IEEE J. Sel. Areas Commun.*, vol. 34, no. 4, pp. 983–997, 2016.
- [46] K. Gao, N. Estes, B. Hochwald, J. Chisum, and N. Laneman, "Power-performance analysis of a simple one-bit transceiver," in *Inform. Theory and Applic. Workshop (ITA)*, 2017.
- [47] K. Gao, J. N. Laneman, and B. Hochwald, "Beamforming with multiple one-bit wireless transceivers," in *Inform. Theory and Applic. Workshop (ITA)*, 2018.
- [48] A. Mezghani, R. Ghiat, and J. Nossek, "Transmit processing with low resolution D/A-converters," in *IEEE Int'l Conf. Electronics, Circuits and Systems-(ICECS'09)*, 2009, pp. 683–686.
- [49] B. Usman, H. Jedda, A. Mezghani, and J. Nossek, "MMSE precoder for massive MIMO using 1-bit quantization," in *IEEE Int'l Conf. Acoustics, Speech and Signal Processing (ICASSP)*, 2016, pp. 3381–3385.
- [50] A. Kakkavas, J. Munir, A. Mezghani, H. Brunner, and J. Nossek, "Weighted sum rate maximization for multi-user MISO systems with low resolution digital to analog converters," in *Int'l ITG Workshop on Smart Antennas*, 2016, pp. 1–8.
- [51] H. Jedda, J. A. Nossek, and A. Mezghani, "Minimum BER precoding in 1-bit massive MIMO systems," in *IEEE Sensor Array and Multichannel Signal Processing Workshop (SAM)*, 2016.
- [52] J. Guerreiro, R. Dinis, and P. Montezuma, "Use of 1-bit digital-to-analogue converters in massive MIMO systems," *Electr. Letters*, vol. 52, no. 9, pp. 778–779, 2016.
- [53] Y. Li, C. Tao, L. Swindlehurst, A. Mezghani, and L. Liu, "Downlink achievable rate analysis in massive MIMO systems with one-bit DACs," *IEEE Commun. Letters*, vol. 21, no. 7, pp. 1669–1672, 2017.
- [54] K. Gao, N. Laneman, and B. Hochwald, "Capacity of multiple one-bit transceivers in a Rayleigh environment," in *IEEE Wireless Commun. and Netw. Conf. (WCNC)*, 2018, pp. 1–6.
- [55] S. Jacobsson, G. Durisi, M. Coldrey, T. Goldstein, and C. Studer, "Quantized precoding for massive MU-MIMO," *IEEE Trans. Commun.*, vol. 65, no. 11, pp. 4670–4684, 2017.
- [56] A. K. Saxena, I. Fijalkow, and A. L. Swindlehurst, "Analysis of one-bit quantized precoding for the multiuser massive MIMO downlink," *IEEE Trans. Signal Processing*, vol. 65, no. 17, pp. 4624–4634, 2017.
- [57] Y. Nam, H. Do, Y.-S. Jeon, and N. Lee, "On the capacity of MISO channels with one-bit ADCs and DACs," *IEEE J. Sel. Areas Commun.*, vol. 37, no. 9, pp. 2132–2145, 2019.
- [58] R. Nikbakht and A. Lozano, "Terahertz transmit beamforming with 1-bit DACs and ADCs," in *European Signal Processing Conf. (EUSIPCO)*, 2021.
- [59] A. Bazrafkan and N. Zlatanov, "Asymptotic capacity of massive MIMO with 1-bit ADCs and 1-bit DACs at the receiver and at the transmitter," *IEEE Access*, vol. 8, pp. 152 837–152 850, 2020.
- [60] E. Torkildson, B. Ananthasubramaniam, U. Madhow, and M. Rodwell, "Millimeter-wave MIMO: Wireless links at optical speeds," in *Allerton Conf. Commun., Control and Computing*, 2006, pp. 1–9.
- [61] E. Torkildson, U. Madhow, and M. Rodwell, "Indoor millimeter wave MIMO: Feasibility and performance," *IEEE Trans. Wireless Commun.*, vol. 10, no. 12, pp. 4150–4160, Dec. 2011.
- [62] X. Song, C. Jans, L. Landau, D. Cvetkovski, and G. Fettweis, "A 60 GHz LOS MIMO backhaul design combining spatial multiplexing and beamforming for a 100 Gbps throughput," in *IEEE Global Commun. Conf.*, Dec. 2015, pp. 1–6.

- [63] C. Lin and G. Y. Li, "Terahertz communications: An array-of-subarrays solution," *IEEE Commun. Mag.*, vol. 54, no. 12, pp. 124–131, Dec. 2016.
- [64] H. Do, N. Lee, and A. Lozano, "Capacity of line-of-sight MIMO channels," in *Int. Symp. Inform. Theory (ISIT)*, 2020.
- [65] A. Lozano and N. Jindal, "Are yesterday's information-theoretic fading models and performance metrics adequate for the analysis of today's wireless systems?" *IEEE Communications Magazine*, vol. 50, no. 11, pp. 210–217, Nov. 2012.
- [66] H. Do, N. Lee, and A. Lozano, "Reconfigurable ULAs for line-of-sight MIMO transmission," *IEEE Trans. Wireless Commun.*, vol. 20, no. 5, pp. 2933–2947, 2020.
- [67] P. Larsson, "Lattice array receiver and sender for spatially orthonormal MIMO communication," in *Proc. IEEE Veh. Technol. Conf.*, May 2005, pp. 192–196.
- [68] B. Wang, F. Gao, S. Jin, H. Lin, G. Y. Li, S. Sun, and T. S. Rappaport, "Spatial-wideband effect in massive MIMO with application in mmWave systems," *IEEE Commun. Magazine*, vol. 56, no. 12, pp. 134–141, 2018.
- [69] B. Wang, F. Gao, S. Jin, H. Lin, and G. Li, "Spatial- and frequency-wideband effects in millimeter-wave massive MIMO systems," *IEEE Trans. Signal Proc.*, vol. 66, no. 13, pp. 3393–3406, 2018.
- [70] R. Blahut, "Computation of channel capacity and rate-distortion functions," *IEEE Trans. Inform. Theory*, vol. 18, no. 4, pp. 460–473, 1972.
- [71] S. Arimoto, "An algorithm for computing the capacity of arbitrary discrete memoryless channels," *IEEE Trans. Inform. Theory*, vol. 18, no. 1, pp. 14–20, 1972.
- [72] R. W. Heath, Jr. and A. Lozano, *Foundations of MIMO Communication*. Cambridge University Press, 2018.
- [73] S. Verdú, "Spectral efficiency in the wideband regime," *IEEE Trans. Inform. Theory*, vol. 48, no. 6, pp. 1319–1343, June 2002.
- [74] R. Nikbakht, A. Jonsson, and A. Lozano, "Unsupervised learning for parametric optimization," *IEEE Commun. Letters*, vol. 25, no. 3, pp. 678–681, 2020.
- [75] T. Haustein and U. Krauger, "Smart geometrical antenna design exploiting the LOS component to enhance a MIMO system based on Rayleigh-fading in indoor scenarios," in *Proc. IEEE Personal Indoor Mobile Radio Commun.*, Sep. 2003, pp. 1144–1148.
- [76] F. Bohagen, P. Orten, and G. Oien, "Construction and capacity analysis of high-rank line-of-sight MIMO channels," in *Proc. IEEE Wireless Commun. Netw. Conf.*, Mar. 2005, pp. 432–437.
- [77] I. Sarris and A. R. Nix, "Design and performance assessment of high-capacity MIMO architectures in the presence of a line-of-sight component," *IEEE Trans. Veh. Technol.*, vol. 56, no. 4, pp. 2194–2202, Jul. 2007.
- [78] C. Sheldon, E. Torkildson, M. Seo, C.P. Yue, U. Madhow, and M. Rodwell, "Spatial multiplexing over a line-of-sight millimeter-wave MIMO link: A two-channel hardware demonstration at 1.2Gbps over 41m range," in *Proc. Eur. Conf. Wireless Technol.*, Oct. 2008.
- [79] H. Do, S. Cho, J. Park, H.-J. Song, N. Lee, and A. Lozano, "Terahertz line-of-sight MIMO communication: Theory and practical challenges," *IEEE Commun. Magazine*, vol. 59, no. 3, pp. 104–109, 2021.
- [80] A. Lozano, A. M. Tulino, and S. Verdú, "Multiple-antenna capacity in the low-power regime," *IEEE Trans. Inform. Theory*, vol. 49, no. 10, pp. 2527–2544, 2003.
- [81] J. Wang, C.-X. Wang, J. Huang, H. Wang, and X. Gao, "A general 3D space-time-frequency non-stationary THz channel model for 6G ultra-massive MIMO wireless communication systems," *IEEE J. Sel. Areas Commun.*, vol. 39, no. 6, pp. 1576–1589, 2021.
- [82] S. Ju, Y. Xing, O. Kanhere, and T. S. Rappaport, "Millimeter wave and sub-terahertz spatial statistical channel model for an indoor office building," *IEEE J. Sel. Areas Commun.*, vol. 39, no. 6, pp. 1561–1575, 2021.
- [83] F. Undi, A. Schultze, W. Keusgen, M. Peter, and T. Eichler, "Angle-resolved THz channel measurements at 300 GHz in an outdoor environment," in *IEEE Global Telecommun. Conf. (GLOBECOM)*, 2021.
- [84] M. T. Ivrlac and J. A. Nosseck, "On MIMO channel estimation with single-bit signal-quantization," in *ITG Smart Antenna Workshop*, 2007.
- [85] Q. Wan, J. Fang, H. Duan, Z. Chen, and H. Li, "Generalized Bussgang LMMSE channel estimation for one-bit massive MIMO systems," *IEEE Trans. Wireless Commun.*, vol. 19, no. 6, pp. 4234–4246, 2020.
- [86] I. Atzeni and A. Tölli, "Channel estimation and data decoding analysis of massive MIMO with 1-bit ADCs," *arXiv:2102.10172*, 2021.